NASA/CR- -96- 208291

Final Report

Turbulence Measurements on a Flap-Edge Model

NASA-Ames University Consortium
NCC2-5140
September 30, 1996

Patrick Moriarty+, Peter Bradshaw+, Brian Cantwell+, James Ross*
+Stanford University, *NASA Ames

Abstract

The properties of hot-wire anemometry were studied using facilities at NASA Ames. Hot-film probes were used because of their durability, but cross-films were limited by non-linear end effects. Hot-film probes were used to measure velocities in the farfield wake of a cylinder with an airfoil in the near-field wake. The airfoil reduced the drag coefficient of the system by 10%. A single wire was used to measure velocity profiles over the top of a NACA 63_2-215 Mod. B wing with a Fowler flap and leading edge slat. Results showed the slat wake remains in the wake over the entire wing. Velocity increased through the slat gap with increased deflection. Slat serrations decreased the chance of separation. Measurements were taken at the flap edge with a single wire. Trends in the data indicate velocity and turbulence levels increase at the flap edge. The porous Revell flap modifies the mean flow near the flap edge. Correlations were made between the hot-wire signal and the unsteady pressure transducers on the wing.

Hot-wire

A majority of the first half of the consortium agreement was spent learning about hot-wire anemometry. Due to a dusty climate in the 7x10 ft. wind tunnel, hot-film probes were considered more reliable than fragile hot-wires. The extra current needed by the hot-films required the use of DISA bridges instead of the Watmuff designed anemometers used in the Fluid Mechanics Laboratory. These also gave a much higher frequency response (50 kHz at 100 m/s) than the Watmuff anemometers. The anemometers allowed much longer cable lengths of 20m. This provided greater freedom of movement of the hot-wires and placement of the anemometers on the outside of the test section.

Considerable effort was made to examine the temperature dependence of the hot-wires. A study using a small calibration tunnel and a space heater was done by performing calibrations at different mean flow temperatures over a 20°C range. Results from this determined that a linear relation between temperature and the calibration coefficients was sufficient.

A calibration study was performed to determine the most effective method of using a King's Law calibration. It was discovered that the slope, intercept and exponent were all functions of the velocity range. In order to approximate a true King's Law, the lowest range of velocities (down to about 4 m/s) had to be included. The entire range of the calibration manometer was used to measure the calibration velocities from 4 m/s to 110 m/s. The velocity at some locations on the wing exceeded this maximum calibration velocity. Therefore, a higher pressure manometer will be used in future tests. Also, the speed and ease of the calibration process will be improved by the use of a pressure transducer instead of a liquid manometer.

In the wind tunnel tests, calibrations were taken twice daily. Error measurements of these calibrations were taken at the end of the day. The maximum error occurring around 100 m/s was approximately 5%. In order to reduce this error, it would be preferable to calibrate the hot-wires in situ.

Cross-wire calibration studies were also performed. The hot-film probes showed non-linearities in their yaw calibration using Bradshaw's[1] method. As pointed out by Bruun[2], this is due to the fact that the hot-film has a thick quartz substrate with a length to diameter ratio of approximately 18. With a small aspect ratio wire, the end effects can have a substantial effect on the lengthwise temperature distribution across the wire. Thus, a nonlinear dependence of heat transfer occurs when yawing the probe. A more desirable length to diameter ratio is around 200. This is the ratio for standard hot-wires. In future tests, a lookup table format will have to be used to calibrate cross-wire hot-film probes. A more sophisticated method using error correction, Cantwell[3], will also be implemented.

HSCT Test

Trial cross-wire measurements were performed on the Boeing HSCT model in the 7x10 ft. wind tunnel. This test was done to demonstrate the robustness of the acquisition software and hardware of the hot-wire system. A modified simultaneous sample and hold device was used to ensure both wires of the cross-wire were sampled at the same time. Unfortunately, a problem caused by the instrumentation cable limited the amount of time spent in the tunnel to three hours. A grid of 20x20 points with half inch spacing was obtained. The resulting velocity map revealed an unexpected flow angularity bias. This was caused by misalignment of the wires in the tunnel and performing the calibration out of situ. Further improvement in software and traverse design should correct these problems. More detailed measurements of the wake were obtained with a seven hole probe survey. Measurements of streamwise turbulence levels showed the same general trends as static pressure losses.

Cylinder Test

In order to gain more experience with the hot-wires in a test situation, measurements were taken during a cylinder experiment directed by Dr. Krothapalli in the 7x10 ft. wind tunnel. The purpose of the experiment was to demonstrate drag reduction of a roughened two-dimensional cylinder by placing an airfoil in the near-field wake. The airfoil was placed about 1.05D downstream of the cylinder and 0.66D off of the centerline (App. A). Reynolds numbers between 1.6×10^5 and 6×10^5 were examined. In order to ensure that the cylinder boundary layer was turbulent at separation, the surface of the cylinder was roughened by a knurling process described by Achenbach[4]. This gave a roughness height of about 100 μm and equivalent sand grain roughness k_s/D estimated at 9×10^{-3}.

One dimensional traverses were made with a single wire across the cylinder wake in the middle of the cylinder span. Output from the hot-wire was converted by a LabVIEW program into mean and RMS velocity profiles. The velocity wakes, Fig. 1, show the total drag of the cylinder is reduced by placing the airfoil in the near-field wake. The mean velocity deficit is less for the case with the airfoil in place. Using seven hole pressure data, a drag coefficient was calculated using conservation of momentum. The calculated drag coefficient for the cylinder alone was 1.09. Adding the airfoil behind the cylinder wake reduced the total drag coefficient by more than 10% to 0.90.

The pressure distribution of the cylinder was measured by pressure taps around the mid-span. Drag of the cylinder alone was calculated from integration of these pressures over the surface. The drag of the system was determined from the combination of cylinder and airfoil drag. The drag of the added airfoil was estimated from Hoerner[5] using a formula for an elliptical cross section. The airfoil was assumed elliptical because of its large thickness, 33%. Hoerner's formula was assumed to give an upper bound on the drag for the airfoil since it is slightly more aerodynamic than an ellipse. The total drag coefficient of the system was calculated from the pressure measurements to be 1.08 for the cylinder alone and 0.95 for the cylinder with the added airfoil in the wake. The drag for the cylinder with airfoil is 5% higher than that calculated from the velocity profiles. The reason for this discrepancy in drag numbers was a change in calibration of the seven hole pressure probes between runs. The static ring was accidentally switched between runs giving a different reference pressure to the seven hole probe system.

An interesting feature of the mean velocity profiles is that they are fairly symmetric in the farfield wake. There is no evidence of the wake of the control airfoil placed in the wake of the cylinder. Examination of a surface pressure profile also shows symmetry around the cylinder itself. This suggests that the added airfoil is a true drag reduction device and does not merely change the direction of the drag force.

The turbulence profiles do have an asymmetrical shape to them. RMS velocities on the airfoil side of the cylinder are less than on the side without the airfoil. Thus, the airfoil must modify the unsteadiness of the vortex shedding without greatly affecting the mean flow. Comparing the wakes to the seven hole probe measurements demonstrated that the turbulence produced was directly related to static pressure losses in the wake. A lower turbulence level resulted in a smaller loss of static pressure. Adding the airfoil decreases the turbulence and static pressure loss in the wake. This again proves the drag is reduced by adding an airfoil to the wake.

The hot-wire output was used to check the shedding frequency of the cylinder both with and without airfoil. The output of the hot-wire was run through an HP spectrum analyzer. The output of the analyzer revealed a narrow band resonant frequency of the vortex shedding. The single wire was placed in the wake 7.5 diameters downstream of the cylinder centerline and 0.66 diameters to the right of the centerline. The measured shedding frequencies were not affected by the presence of the airfoil. The Strouhal number remained constant around 0.2.

One Dimensional Traverse

Because the present traverse in the wind tunnel did not provide adequate access to the top of the wing, a new traverse had to be built in order to access the areas of interest. The first idea was to build a traverse which could hold hot-wires on the model itself. This was ruled out because of the cost of the modifications to the model and the lack of space to run instrumentation cable. The next best solution was to traverse from the side-wall of the tunnel which corresponded to the top of the wing.

This traverse was to be cantilevered and able to reach as far as the bottom surface of the deflected flap. The traverse consisted of a hollow circular cylinder (1 in. dia.) with an adapter at the end. The adapter allowed any type of Dantec hot-wire mount to be screwed in, single or cross-wire (Fig. 2). The hot-wire mount could be extended an additional four inches in order to reduce the effect of the traverse cylinder on the flow around the hot-wire.

Because of the possibility of flow induced vibrations of the cantilevered section with cylindrical cross-section, an airfoil fairing was placed around the cylinder for the first three feet extended from the wall. A nylon bushing at the end of the airfoil section kept the cylinder in the center of the airfoil. Wrapping wire around the cylinder was also considered in order to break the vortex shedding of the exposed cylindrical section. Testing of the wire wrap showed no further decrease of the amount of vibration and was deemed unnecessary. The section of the traverse inside the tunnel is shown in Fig. 3.

The traverse section of the outside of the tunnel, Fig. 4, consisted of a set of guide rails and a lead screw attached to a DC motor. A set of linear bearings attached to a plate was used to attach the traverse cylinder to the guide rails. The pipe fittings holding the traverse cylinder to the plate could be loosened to allow rotation of the hot-wire in the flow, giving it effectively two degrees of freedom. A cross-over switch was used to alternate the direction of the current so that the motor could be driven both forward and backwards. Using the switch would drive the cylinder into or out from the test section.

During the flap edge test, a straight single wire was used to take the two dimensional cross-section data. However, the friction bearings of the Dantec probe holders were not strong enough to hold the hot-wire in a position parallel to the flow. Thus, a passive aerodynamic fin was placed on the back of the hot-wire holder, Fig. 5. The fin proved effective in keeping the hot-wire pointed into direction of the mean flow. It was not used in the flap tip region because the size of the fin was on the order of the size of the vortex. The wire would not have remained in a correct orientation with the flow off of the flap edge.

A custom wind tunnel wall section was cut to access various points on the top of the wing. The traverse and airfoil fairing were bolted to the wall at the different locations for measurement. Three different spanwise locations were cut for examining the slat. A long section was cut out of the wall to allow movement along the entire top section of the wing. Finally, a wide section was cut out near the flap edge. For repeatability, positions were marked by tracing the inner tunnel plate on the wall with a wax pen. Repeatability error was estimated to be 1/32 inch.

Positioning error in the traverse was a large concern. It was discovered that the lead screw mechanism had an error of about 1/16". The major positioning error came from a steady state aerodynamic deflection of the cantilevered cylinder while the tunnel was running. The maximum deflection of the probe was estimated to be 0.25" perpendicular to the traverse plane. This was fairly consistent, however, such that the repeatability error was much less than this. The error mostly affected the absolute position of the probe near the flap edge.

Unsteady fluctuations of the probe were also a concern in the flap edge area. The peak to peak fluctuations of the probe were estimated to be 1/8" when the cylinder was in the core of the vortex. These fluctuations also caused false turbulence levels. False turbulence levels were prominent when making measurements on the bottom side of the flap because the traverse cylinder was close to the turbulent vortex core. When this occurred RMS velocities increased by about 4%.

Errors in traverse positioning proved to be the dominant error source. These errors were not critical in the two dimensional profiles of the top of the wing. During these traverses only the vertical position was crucial. The repeatability of vertical position was within the error range of the traverse - around 1/32 inch. The spanwise and chordwise position were also fairly good - around 1/32" as well. Oscillations of the probe were also considerably less because the traverse was not directly placed in the tip vortex.

Also, the small winglet place on the probe to control its pitching moment served to dampen out the aerodynamic vibration. It was estimated that the maximum vibration displacement during the two dimensional traverses was around 1/16". This occurred during measurement behind the flap gap.

Flap Edge Test Setup

Measurements were taken in the 7 ft. by 10 ft. wind tunnel of NASA Ames. The model consisted of a NACA 63_2-215 Mod. B main element with a half span 30%c Fowler flap and a 15%c LB-546 slat (App. A). Mounted vertically between two false walls, the model had a span of 5 feet and a clean (flap stowed) chord of 2.5 feet. On the main element, boundary layer trip strips were placed at 5% and 10%c on the upper and lower surfaces, respectively. The test Mach number remained constant at 0.22 with a Reynolds number based on chord of 3.7 million. The turbulence intensities of the empty test section were measured to be 0.14%, 0.30% and 0.34% for u, v, and w respectively. Approximating a landing configuration, the angle of attack for the wing was fixed at 10° and the flap angle was set to 39°. The slat angle was varied between 6° and 26° and the slat was completely removed for flap edge measurements.

Flap-Edge Measurements

Measurements of the velocities were taken in the three dimensional flow field of the flap edge as well as the more two dimensional profiles over the top of the wing itself (App. A).

Temperature variation throughout the tunnel was a problem for the hot-wires. A temperature difference of approximately three degrees Celsius was measured between the top and bottom of the tunnel. There were also pockets of hot and cold spots in the same position of the tunnel which varied at most 1.5 degrees Celsius. Temperature variation between the center of the vortex and the surrounding flow was also considered a problem. Taking this into consideration, a linear temperature dependence was included in both the calibration and acquisition software. A thermocouple was placed behind the hot-wire in the flow and the temperature was recorded at every data point.

The sample period for all measurements was kept constant at 20 seconds. The sampling rate was 1000 Hz. The period was long enough to obtain a fairly stable mean in very turbulent flow and also obtain accurate RMS velocities. The raw hot-wire signal was passed through an anti-aliasing filter with a cutoff frequency of 50 kHz and a roll-off rate of 18 dB/decade.

Time dependent data was necessary for correlation with unsteady pressure transducers and wall microphones. However, only the AC coupled signal was needed. The hot-wire signal was passed through a high pass filter with a DC cutoff frequency of 1 Hz and a roll-off rate of 18 dB/octave. This signal was then recorded on a Metrum digital recording tape along with the signals of 14 Endevco pressure transducers and one wall microphone. The sample rate of the Metrum was set at 80 kHz with its anti-aliasing filter set at 20 kHz. These numbers were chosen by the acoustic levels previously measured. Nothing above 20 kHz was deemed acoustically interesting. The hot-film probes were tuned to a frequency response of approximately 50 kHz (at 100 m/s). Thus, all frequencies up to 25 kHz were accurately captured by the hot-film probe. The digital recorded tape was later played back and analyzed on an HP Spectrum Analyzer. Correlations were made between the hot-wire and the unsteady pressure sensors, but will not be covered in this paper.

Top of the Wing Results

The two dimensional profiles over the top of the wing proved to be most interesting. Four different configurations were examined: no slat, 10° slat deflection, 20° slat deflection and 20° slat deflection with a serrated trailing edge. The actual slat deflection angles were closer to 6 degrees and 26 degrees respectively. The slat gap was fixed at 2% of wing chord. The overlap was -0.5%c.

The traverse at 0.66 of the slat chord, Figure 6, shows that the mean velocities remain relatively unchanged over the slat when varying the slat angle. The 10 deg. slat case shows slightly higher turbulence levels. This is because the relative position of the probe is different between the 20° slat and the 10° slat. For the measurements of the 20° slat, the probe is actually farther back chordwise on the slat than 10° slat. Both of these turbulence levels are the order of the freestream turbulence ~1%.

Traverses just behind the slat gap, 0.05 of the main chord, Figure 7, show a difference in velocity profiles between configurations. The mean velocities of the 20° slat case are nearly 10% higher than the 10° slat case. The no slat case has the highest velocities of all - 5% greater than the 20° slat. This is consistent with surface pressure plots of the 10° and 20° slat which show the 20° slat has a higher pressure peak on the main element. The 20° slat gap flow has a much higher jet velocity than the 10° slat and therefore a higher main element pressure peak. Repeated runs showed that turbulence levels were relatively independent of the slat deflection. The wake of the slat can be seen in all of the mean velocity profiles as well as the turbulence levels.

Velocity profiles near the center of the main element, Figure 8, show close similarity in all model configurations. There is slight evidence of the slat wake with a deficit in the mean velocity and an increase of the turbulence levels at about 4% chord from the surface. This is more pronounced in the 10° slat than the others. The reason for this is explained below.

Mean velocities near the main trailing edge, Fig. 9, are once again fairly similar. Again, the 10° slat wake is slightly larger than the 20° slat wake.

The effect of slat deflection is much more pronounced in the wakes behind the flap gap. Figure 10 shows the velocity profiles at 0.16 of the flap chord. The slat wake can be seen in all of the slat configurations around 8%c from the surface. It is most pronounced for the 10° and basic 20° slats. There are appreciable differences in velocities at this location. A higher slat deflection angle produces a lower velocity peak. This is because the slat increases the camber of the wing. On the backside of the wing the adverse pressure gradient is larger with increased curvature. Therefore, the flow is decelerated over the top of the wing. The serrated slat configuration also has slightly less velocity deficit from the top of the wing than the basic slat. This is likely cased by the serrations increasing the turbulence in the boundary layer. The more turbulent boundary layer is less affected by the adverse pressure gradient and maintains a more robust profile. The lesser evidence of a slat wake is also due to this increased mixing. The turbulence profile of the no slat case shows abnormally high turbulence levels outside of the wake. This was caused by a faulty wire introducing electrical fluctuations into the system. The wire was quickly replaced, but time constraints did not permit a repeat run.

Just past half chord of the flap, Figure 11, the velocity profiles are similar again. Velocities for the 20° slats are again slightly lower because of the greater adverse pressure gradient. The 20° slats have higher turbulence levels in the wing wake. All slat configurations show the wake of the slat starting at 10%c from the surface and ending at about 15%c from the surface.

The final two dimensional velocity profiles, Figure 12, were taken at the trailing edge of the flap. These profiles again show very good agreement with the previous data. The 20° slat configuration has lower velocities and higher turbulence levels. The basic 20° slat was separated, as evidenced by 80% turbulence levels, in the wake. This was probably induced by the hot-wire probe or traverse at the trailing edge. Previous runs without the hot-wire did not indicate any kind of separation. The serrated 20° slat did not separate. This demonstrates that the serrations increased the turbulence in the boundary layer and helped prevent separation.

An interesting phenomena occurs in all turbulence profiles over the flap. The 20° slats have higher turbulence levels in the wing wake, while the 10° slat has lower turbulence levels than even the no slat case. The reasons for this are not fully understood. One possible reason is that the 10° slat is configured such that the jet velocity and the flow velocity over the top of the slat are nearly equal, Fig. 7. Therefore, the turbulence created in the shear layer of the slat gap is not as great.

Flap Edge Results

The three dimensional flow region of the flap edge was much harder to measure accurately with a single wire, as made evident by the wide scatter in the data. However, trends in the data do reflect some of the flow physics. A single wire with a 90° bend, Fig. 2, was used for measurements in this region. The probe was oriented such that it would measure the freestream velocity assuming no sideslip. The probe could be rotated to measure velocity in a plane parallel to the wing chord. However, any out of plane velocities could not be measured directly even though they did affect the hot-wire output. At each measurement point, the probe was rotated by hand to the point of maximum velocity. This done by reading the point of maximum voltage with a voltmeter. The next phase of the test will implement an automatic control of this procedure as well as the ability to pitch and yaw the probe.

Traverses were made in relation to unsteady pressure transducers on the flap edge. The zero location was directly to the side of the flap edge transducers about 3/8". Traverses were then made in a line perpendicular to the flap chord on both the top and bottom of the flap. Three different chordwise positions were examined at 40%, 53%, and 68% of the flap chord. Measurements were taken on two different flap configurations: the standard composite Fowler flap and a porous tip Fowler flap designed by Revell[6] for noise suppression.

Figure 13, shows the velocity profiles at 40% of the flap chord. It is obvious that the point of maximum total velocity is at the flap tip (zero on the plot). The point of minimum velocity corresponds to the wake of the main element. Examining the turbulence levels shows a similar two peak pattern. The point of maximum turbulence is the main element wake. A much smaller peak at the flap edge indicates that the vortex rollup over the edge is fairly steady in this area. Comparison between the porous and regular flap tip show very little difference in mean flow or turbulent fluctuations.

Figure 14 displays the velocity profiles slightly farther downstream at a location of 53% of the flap chord. The mean velocity shows a similar pattern of low velocity in the wake of the main element and a high velocity at the flap edge. There is also good agreement between the regular and porous tip flaps. Plots of the turbulence intensity show a slight difference between the two configurations. Both show a high peak at the flap edge. However, the regular composite flap has a much higher peak turbulent intensity of 15%, compared to only 5% for the porous tip.

Figure 15 shows velocity profiles farther downstream at 68% of the flap chord. Here the difference between the porous and regular flap tips is more pronounced. The mean velocity of the regular tip reaches a peak similarly to the previous profiles. However, the porous tip flap mean velocity increases near the flap edge and then levels off. This plateau continues for a couple of main chord percentages and then increases again to a lower level than the regular tip peak. The mean velocity of the porous tip then seems to follow the profile of the regular tip once past the influence of the flap. The turbulence levels are also significantly different. The peak of the porous tip flap is over twice as high as that of the regular flap. These facts suggest that the porous tip flap actually modifies the vortex structure around the flap edge.

One final conclusion made from these plots is that the vortex does not follow the flap edge. Its center corresponds to the point of maximum mean velocity and moves farther away from the flap edge as it convects downstream. This observation is consistent with the flow visualization studies of the wing.

Conclusions

The HSCT test revealed that more research will have to be done on using cross-film probes. An alternate method of calibration will be used and a more effective method of placing the probes in the direction of the flow must be implemented.

The cylinder test demonstrated that the drag of a cylinder can be reduced by placing an airfoil in the near-field wake. Mean velocity data from the hot-wire can be used in conjunction with static pressure data of the wake to produce reasonable drag coefficients.

Measurements of the quasi-two-dimensional flow over the top of the wing revealed a great influence of the slat deflection. The slat wake could be seen in all velocity profiles and continued over the flap. Higher slat deflections produced a higher jet flow speed through the slat gap. This resulted in a greater suction peak on the main element. Serrations of the flap increased the turbulence in the boundary layer. This made the wing less likely to separate and increased flow velocities over the flap.

Measurement of the three dimensional flow about the flap edge was difficult to resolve with a single wire. Trends in the data indicate the flap tip is a local point of maximum velocity and turbulent intensities. The porous Revell flap tip used for acoustic damping changed the structure of the vortex around the flap edge. Further studies will be made to further map out this region's velocities and turbulence.

Uncertainty of the position near the flap edge was not at all reasonable. For the next phase of the test a new traverse mechanism will have to be used. One approach would be to use an electronic touch sensor to find the surface while the tunnel is running as done by Chow, Zilliac, and Bradshaw[7]. Aerodynamic deflection of the traverse can then be trimmed by moving the traverse back to the desired position near the surface. A

three dimensional traverse will be needed to traverse the probe to any position on the edge. Because the next phase of the experiment will be to map the flow field three dimensionally, the probe should also have the ability to pitch and yaw. The probes can then be oriented in a direction which would reduce their error from cross-flow velocity components. Another option is to mount the hot-wires to the flap and/or wing itself and traverse them from the surface. This would cure the problem of probe vibration, but increases the complexity of the flap design.

References

[1]Bradshaw, P. "Cross-wire probe calibration," Heat Transfer and Turbulence Mechanics Group, M.E. Dept., Stanford University, Stanford, CA, July 1992.

[2]Bruun, H. H., Hot-wire Anemometry - Principles and Signal Analysis, Oxford Science Publications, New York, 1995.

[3]Cantwell, B. "A flying hot-wire study of the turbulent near wake of a cylinder at a Reynolds number of 140,000," Graduate Aeronautical Laboratories, California Institute of Technology, Pasadena, CA, 1976.

[4]Achenbach, E., and Heinecke, E. "On vortex shedding from smooth and rough cylinders in the range of Reynolds numbers $6x10^3$ to $5x10^6$," *Journal of Fluid Mechanics*, 1981, pp. 109, 239-251.

[5]Hoerner, S.F., Fluid Dynamic Drag, Hoerner Fluid Dynamics, Albuquerque, NM 87120, 1965, pp. 3-1 - 3-28.

[6]Revell, J., Kuntz, H., Balena, F., "Airframe trailing edge flap noise reduction by porous acoustic treatment," 3rd AIAA/CEAS Aeroacoustics Conference, Atlanta, GA, May, 1997.

[7]Chow, J. S., Zilliac, G. G., Bradshaw, P., "Turbulence measurements in the near-field of a wingtip vortex," ASME Forum on Turbulence in Complex Flow, Nov. 6-11, 1994, Chicago, Illinois.

[8]Storms, B. L., Takahashi T. T., Ross, J. C., "Aerodynamic influence of a finite-span flap on a simple wing," SAE Technical Paper Series - 951977, 1995.

[9]Mathias, D. L., Roth, K. R., Ross, J. C., Rogers, S. E., Cummings, R. M., "Navier-Stokes analysis of the flow about a flap edge," AIAA-95-0185, 1995.

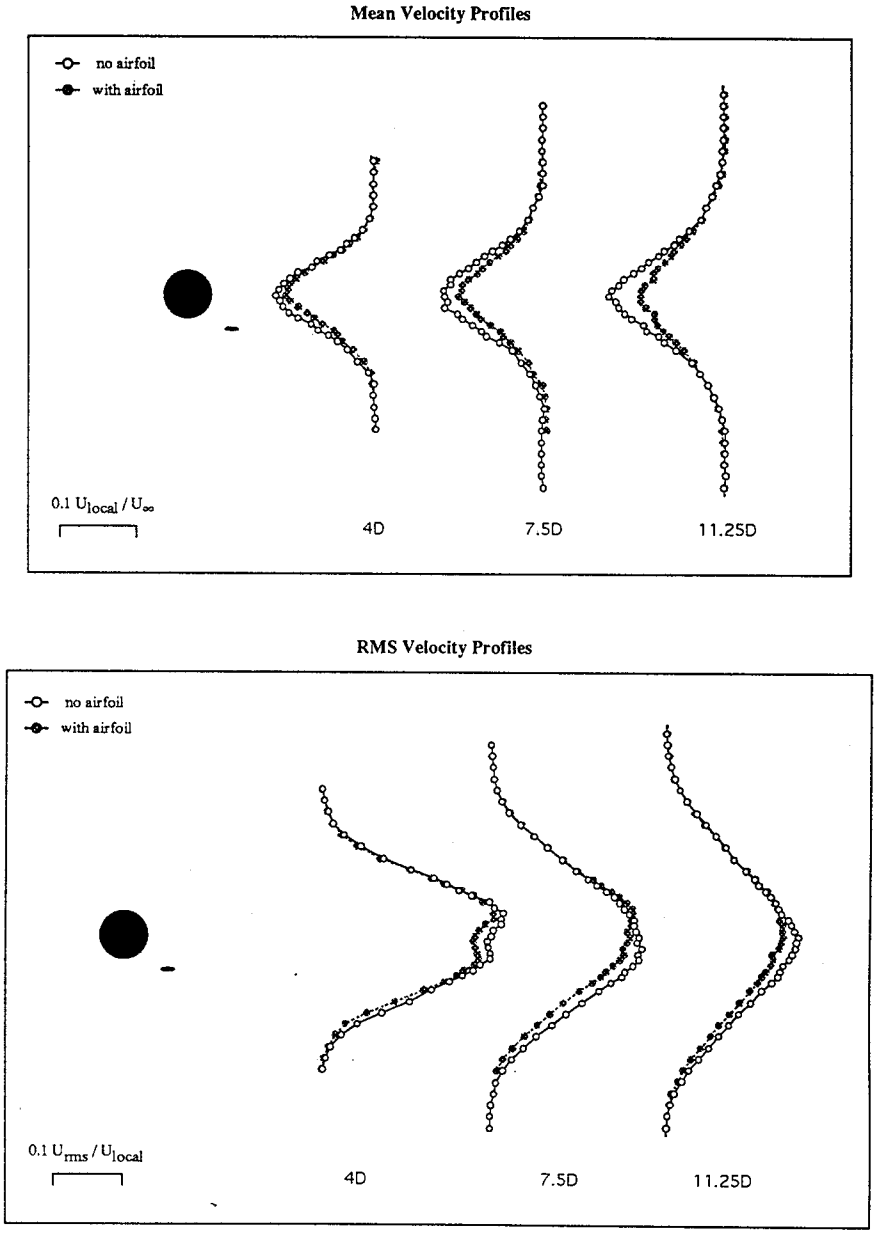

Figure 1. Cylinder Velocity Profiles

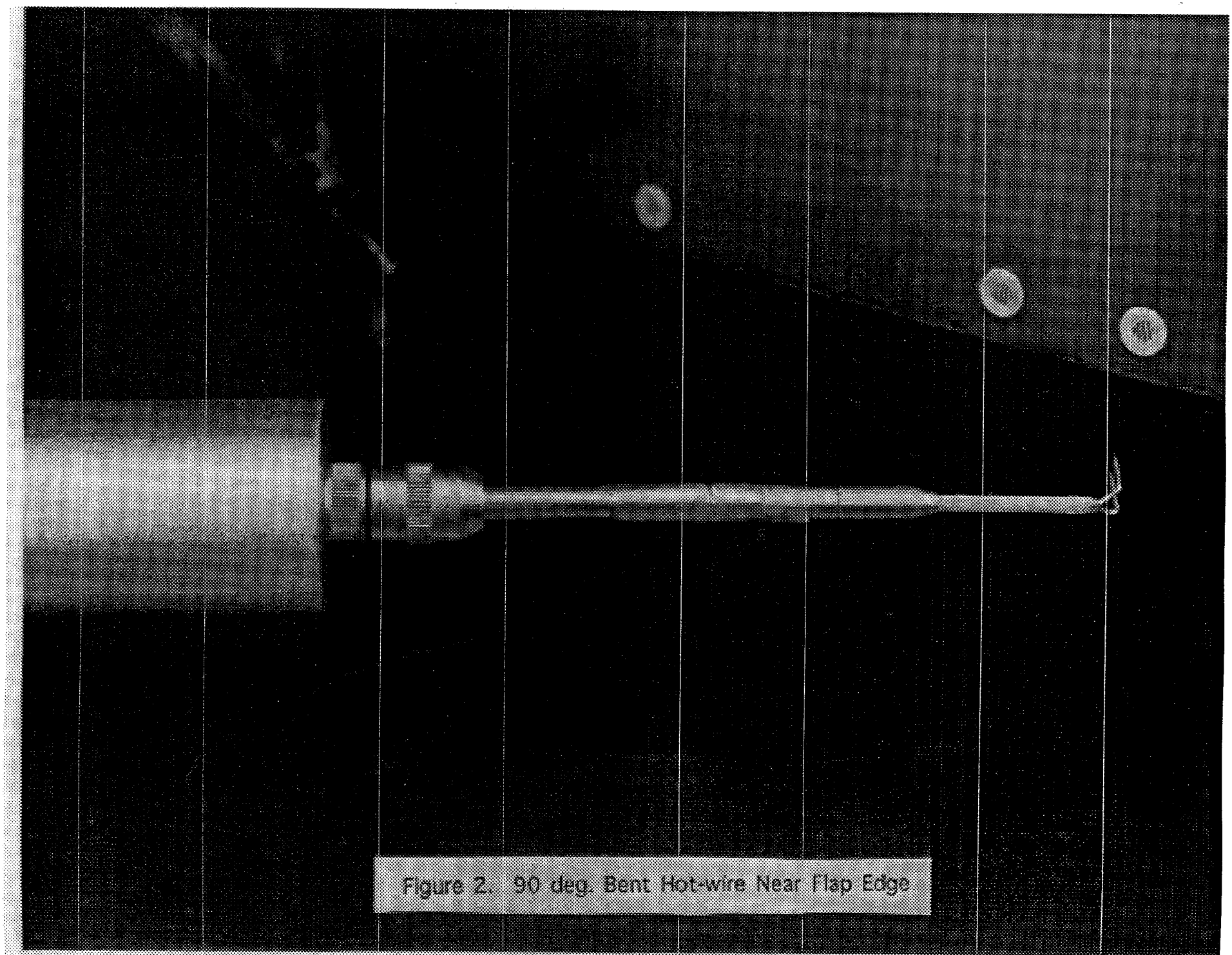

Figure 2. 90 deg. Bent Hot-wire Near Flap Edge

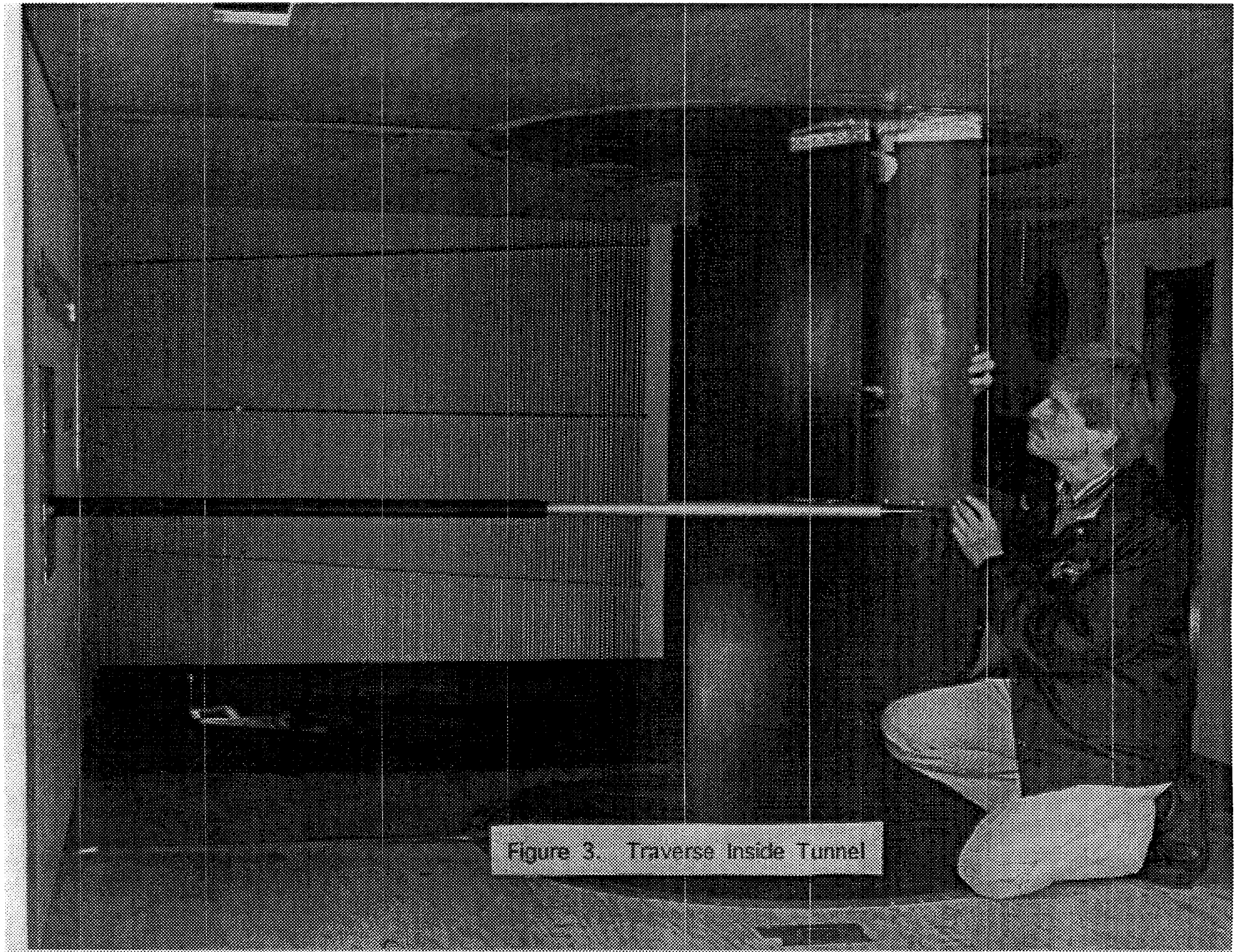

Figure 3. Traverse Inside Tunnel

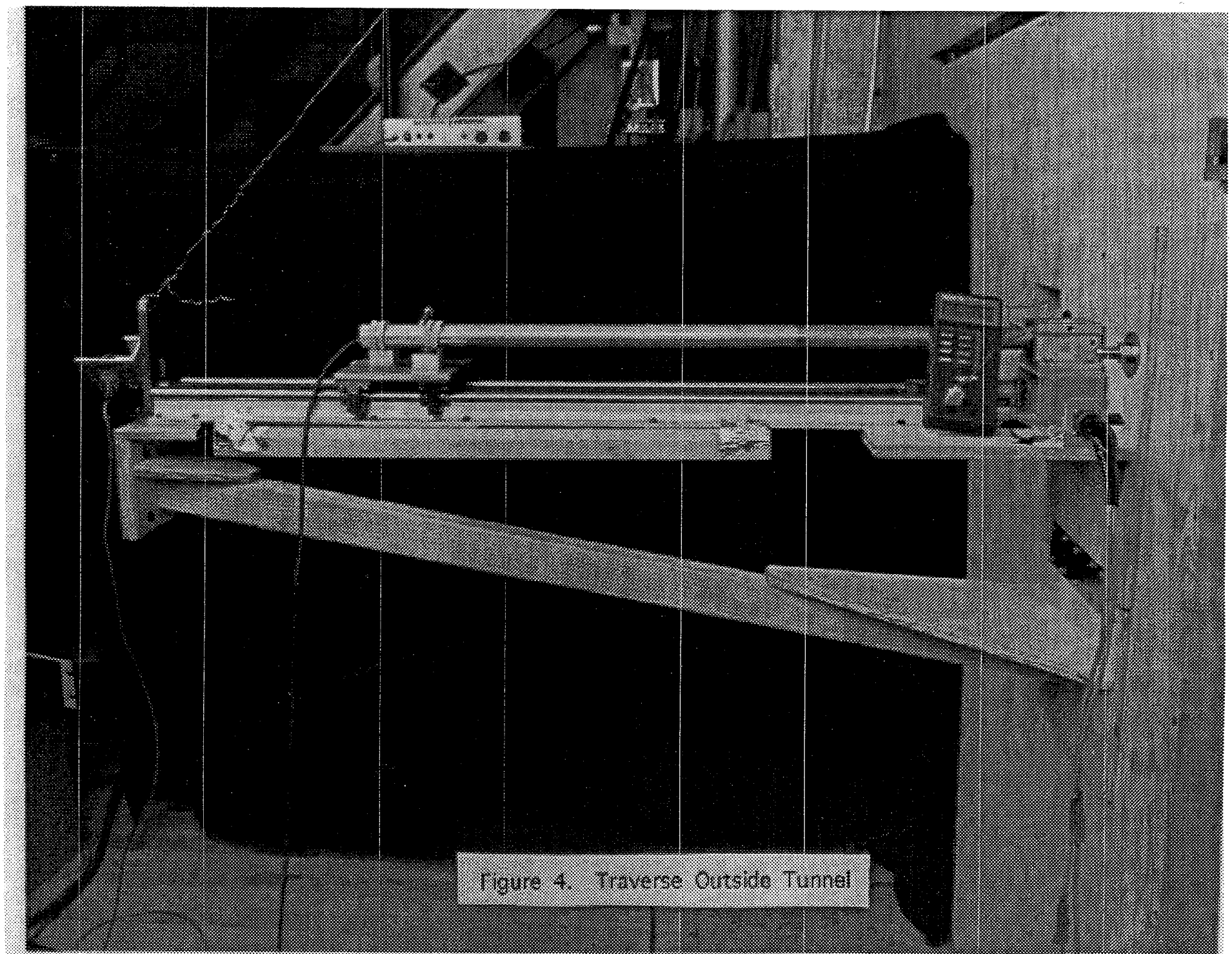

Figure 4. Traverse Outside Tunnel

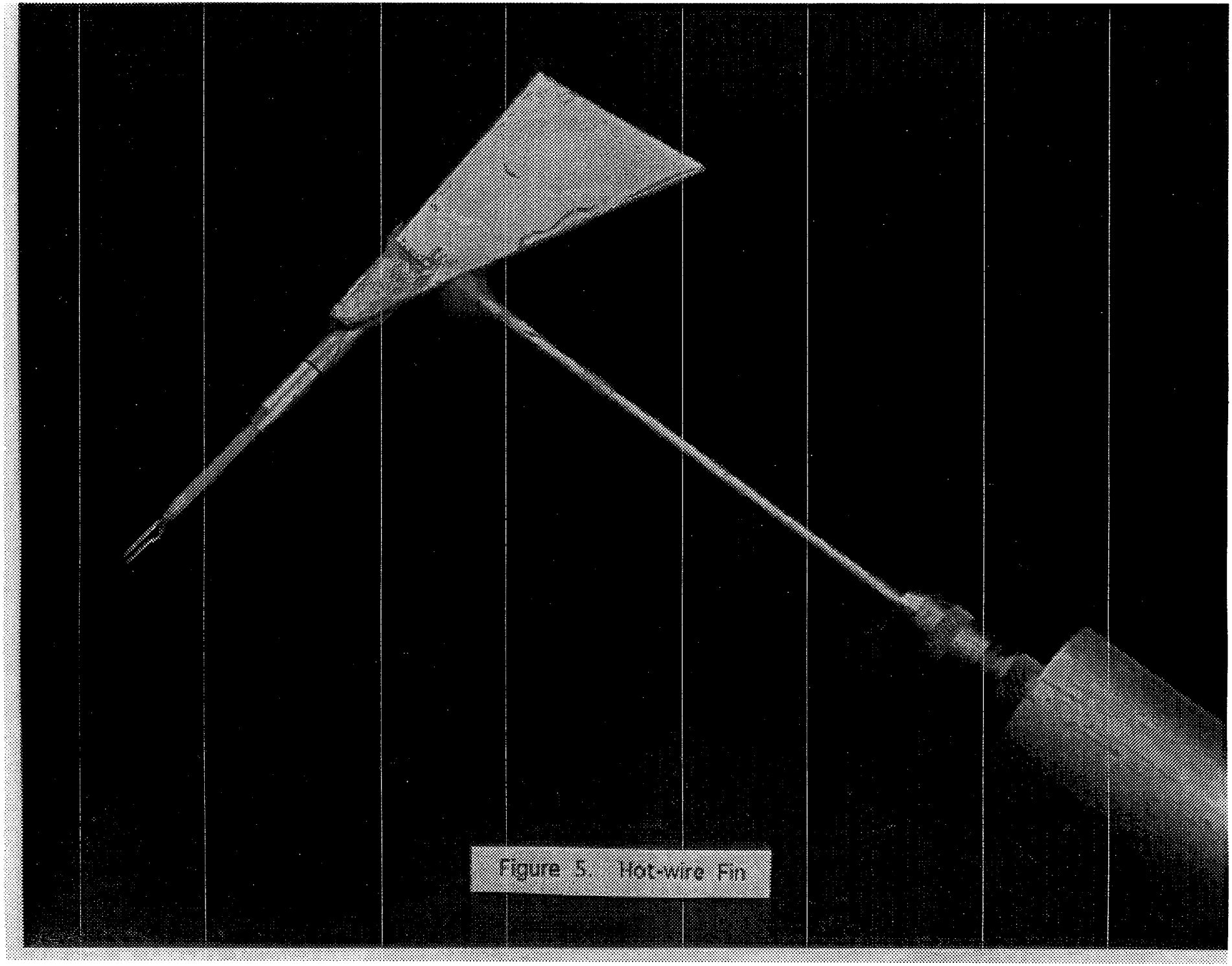

Figure 5. Hot-wire Fin

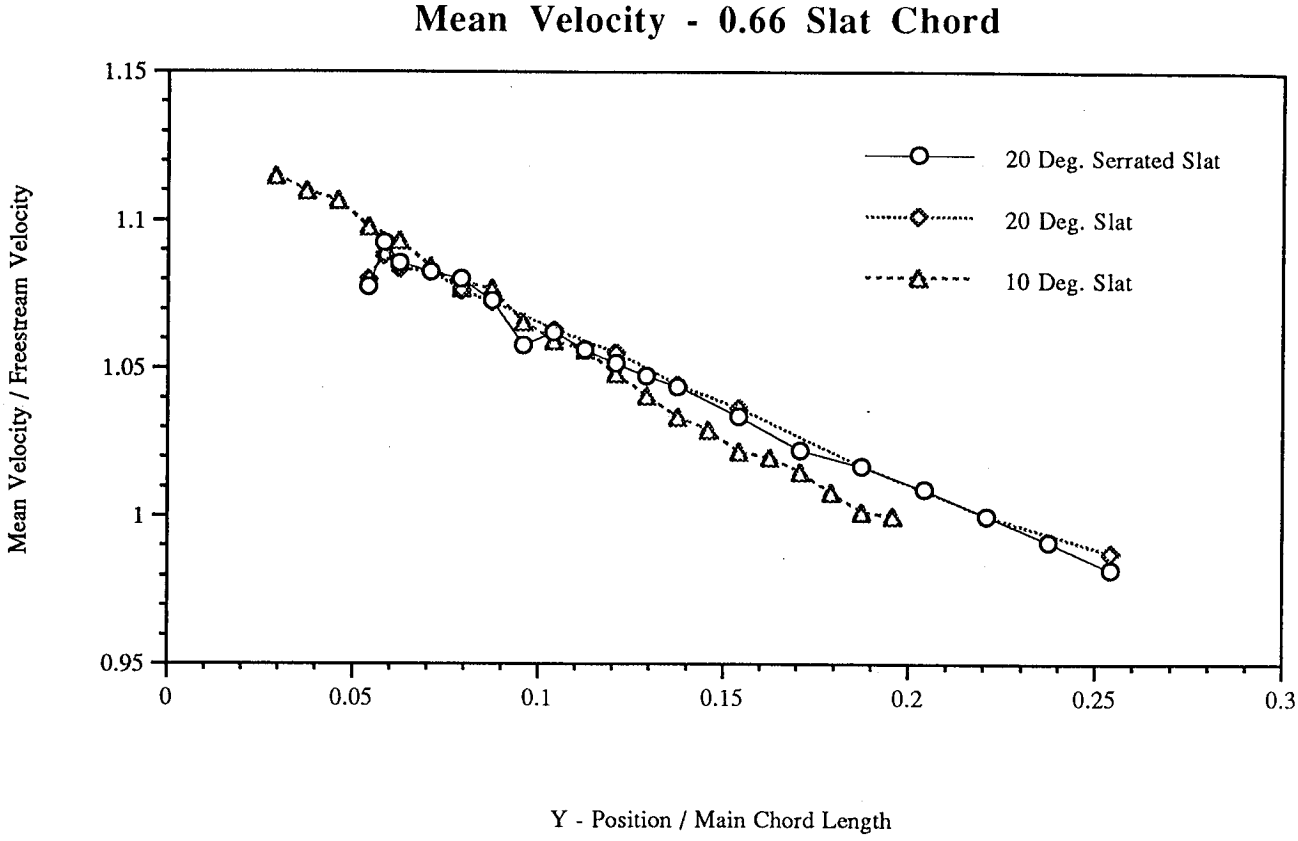
Mean Velocity - 0.66 Slat Chord
Mean Velocity / Freestream Velocity
1.15
1.1
1.05
1
0.95
0
0.05
0.1
0.15
0.2
0.25
0.3
20 Deg. Serrated Slat
20 Deg. Slat
10 Deg. Slat
Y - Position / Main Chord Length

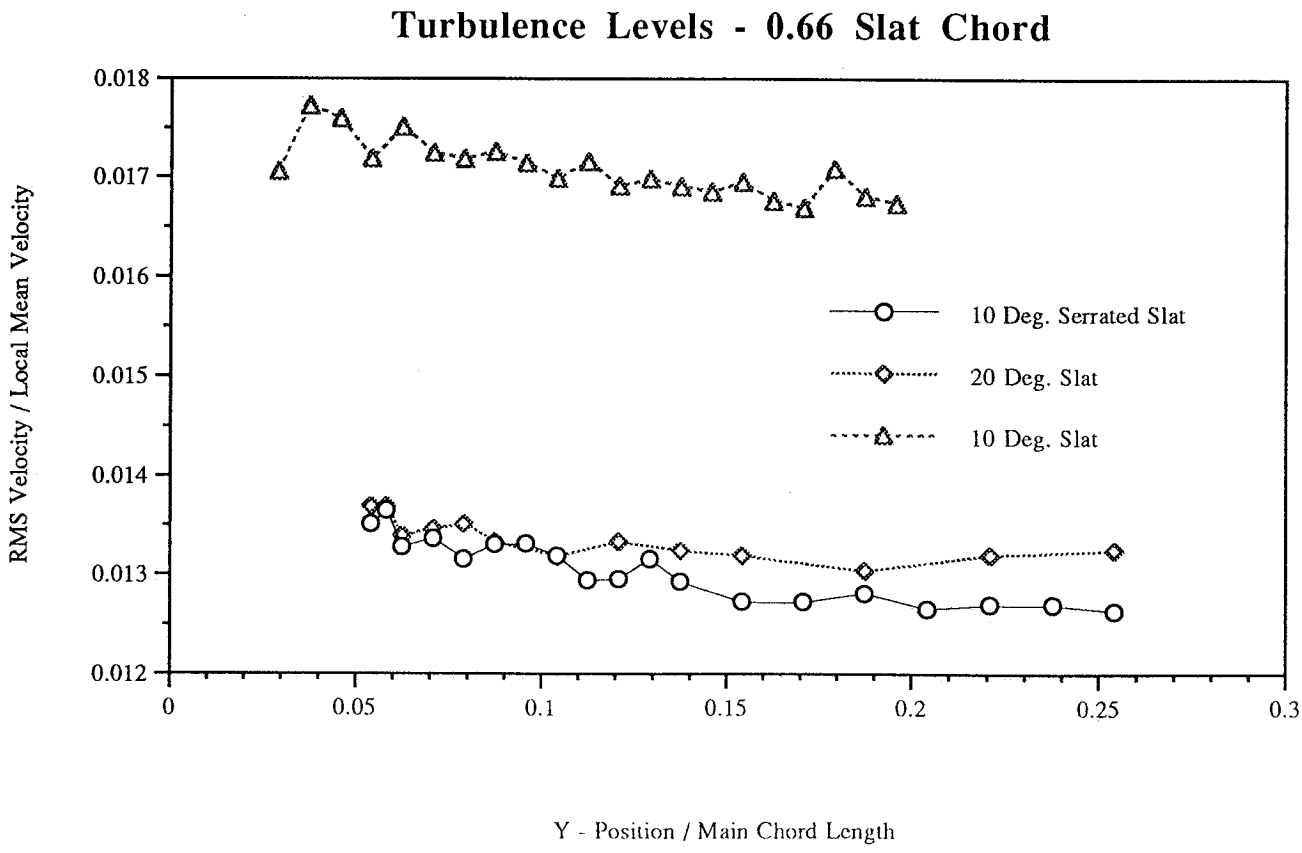
Turbulence Levels - 0.66 Slat Chord
RMS Velocity / Local Mean Velocity
0.018
0.017
0.016
0.015
0.014
0.013
0.012
0
0.05
0.1
0.15
0.2
0.25
0.3
10 Deg. Serrated Slat
20 Deg. Slat
10 Deg. Slat
Y - Position / Main Chord Length

Figure 6

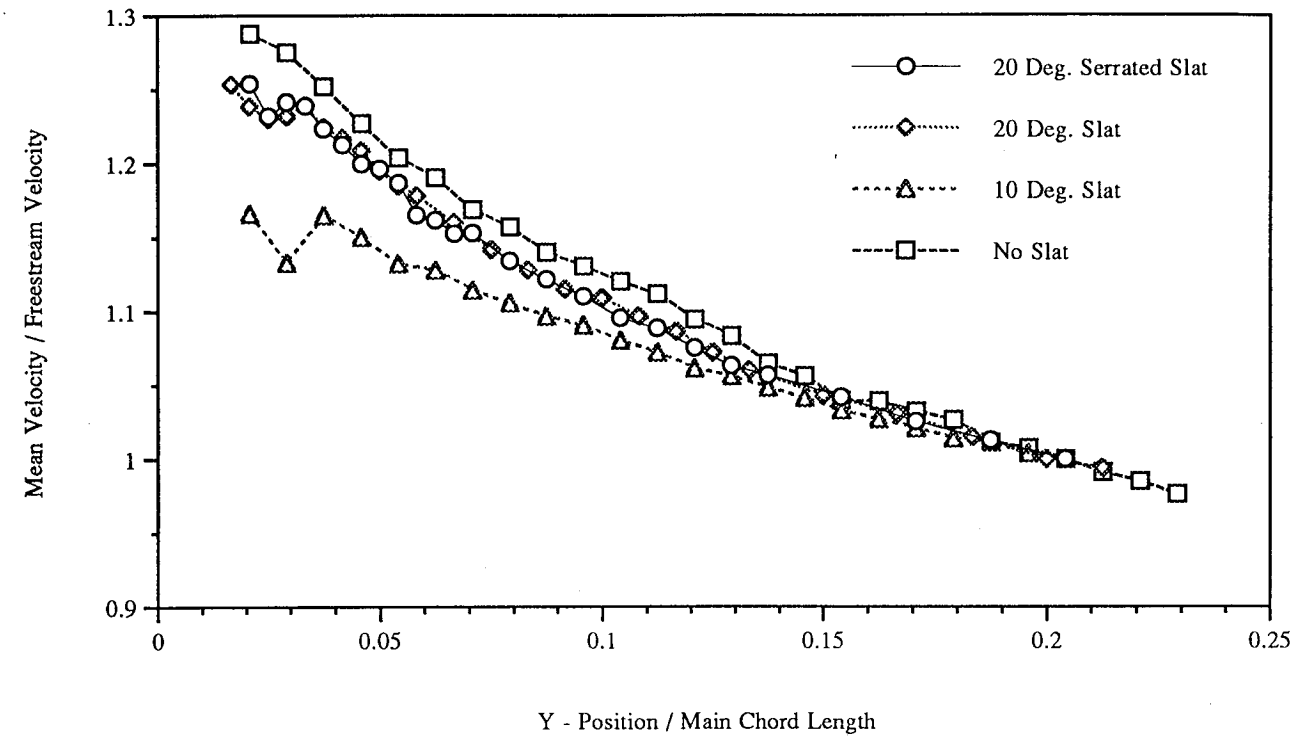
Mean Velocity - 0.05 Main Element Chord
Mean Velocity / Freestream Velocity
1.3
1.2
1.1
1
0.9
0
0.05
0.1
0.15
0.2
0.25
20 Deg. Serrated Slat
20 Deg. Slat
10 Deg. Slat
No Slat
Y - Position / Main Chord Length

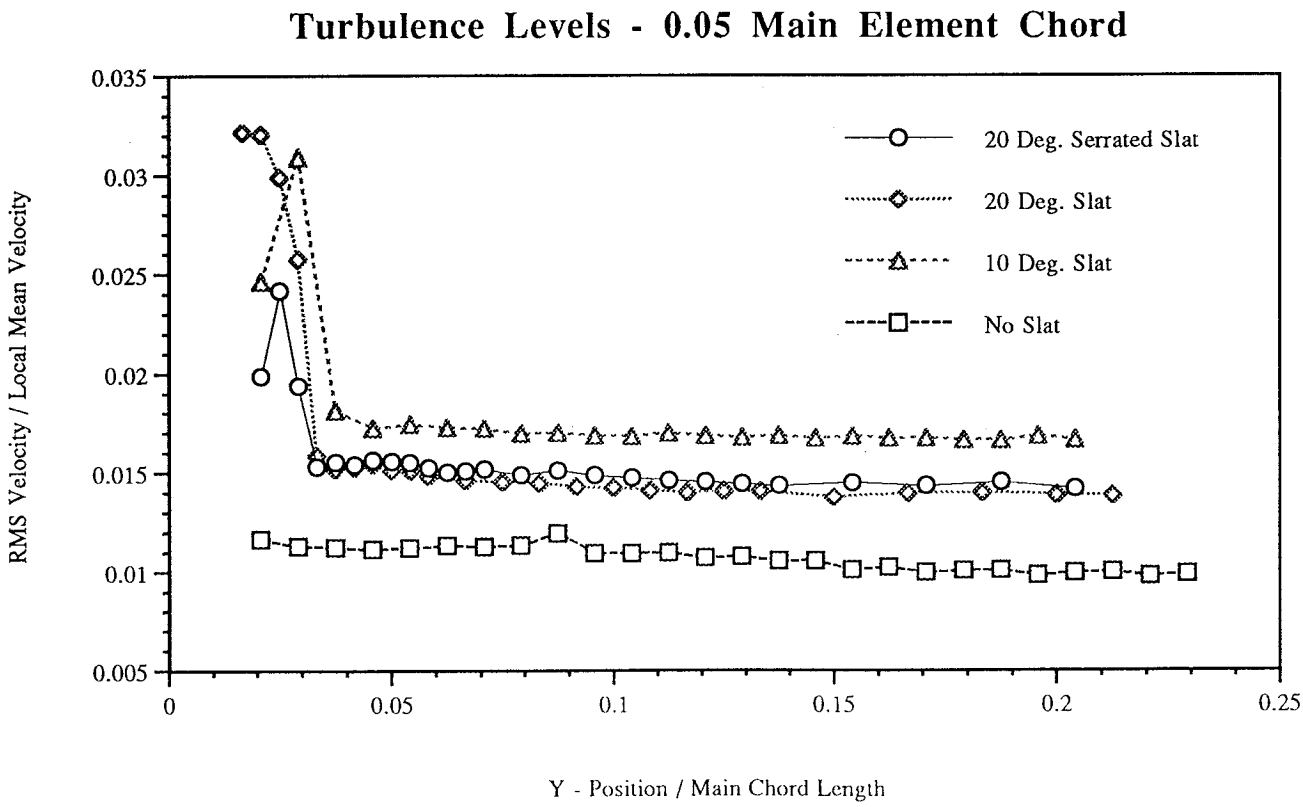
Turbulence Levels - 0.05 Main Element Chord
RMS Velocity / Local Mean Velocity
0.035
0.03
0.025
0.02
0.015
0.01
0.005
0
0.05
0.1
0.15
0.2
0.25
20 Deg. Serrated Slat
20 Deg. Slat
10 Deg. Slat
No Slat
Y - Position / Main Chord Length

Figure 7

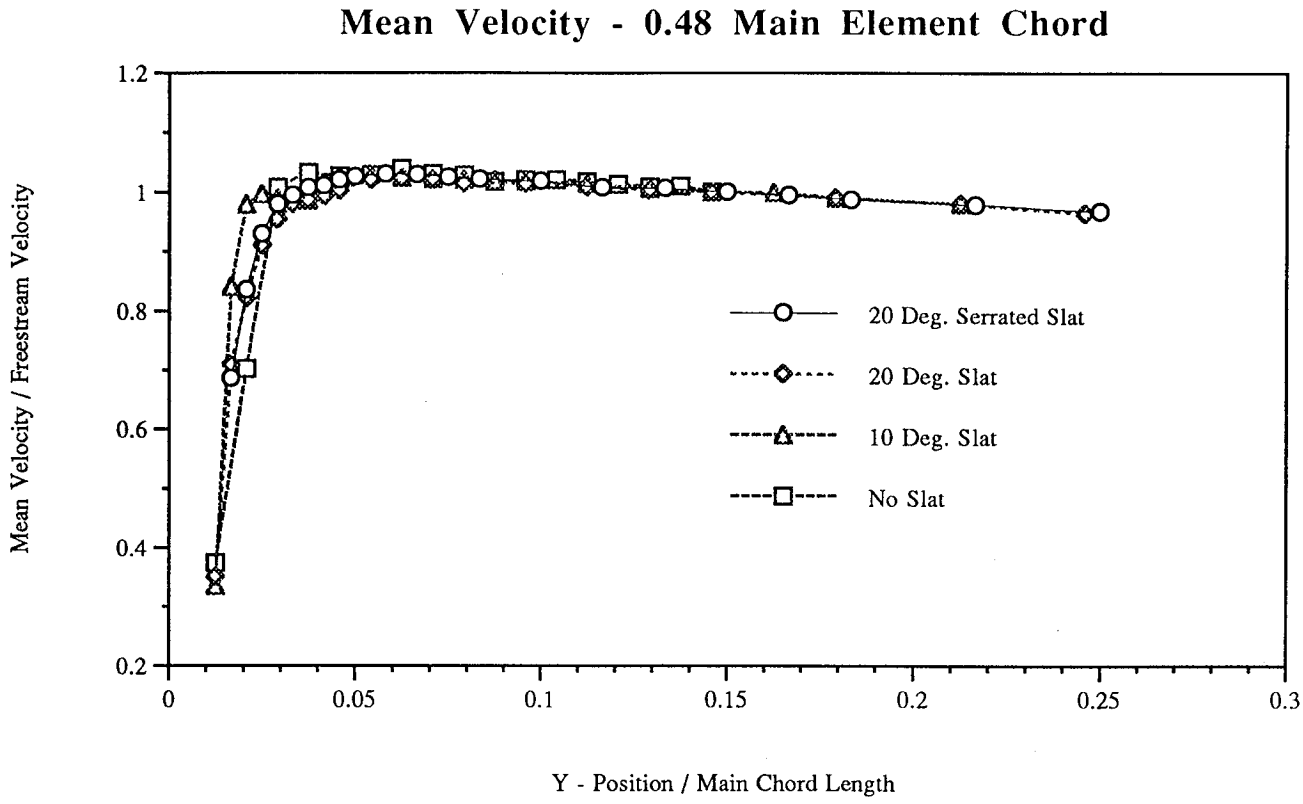
Mean Velocity - 0.48 Main Element Chord
Mean Velocity / Freestream Velocity
1.2
1
0.8
0.6
0.4
0.2
0
0.05
0.1
0.15
0.2
0.25
0.3
20 Deg. Serrated Slat
20 Deg. Slat
10 Deg. Slat
No Slat
Y - Position / Main Chord Length

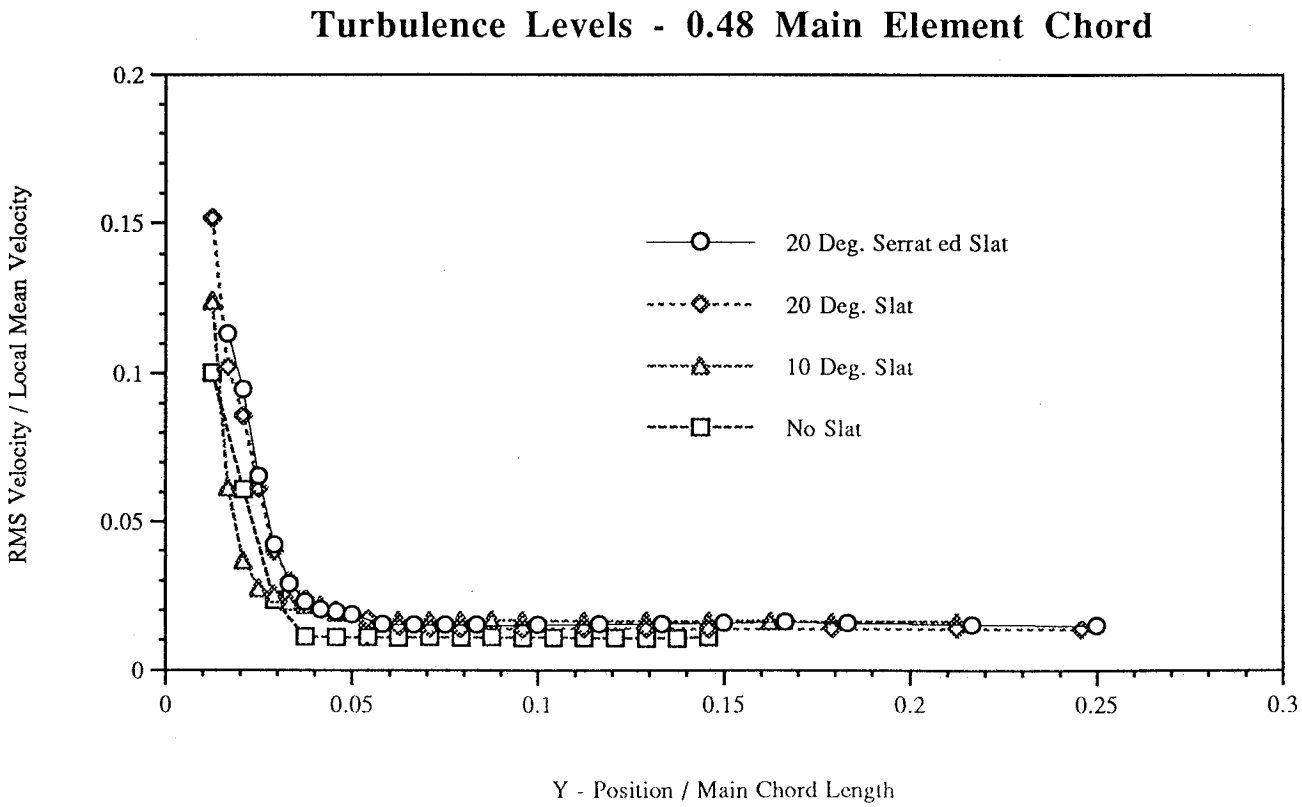
Turbulence Levels - 0.48 Main Element Chord
RMS Velocity / Local Mean Velocity
0.2
0.15
0.1
0.05
0
0.05
0.1
0.15
0.2
0.25
0.3
20 Deg. Serrat ed Slat
20 Deg. Slat
10 Deg. Slat
No Slat
Y - Position / Main Chord Length

Figure 8

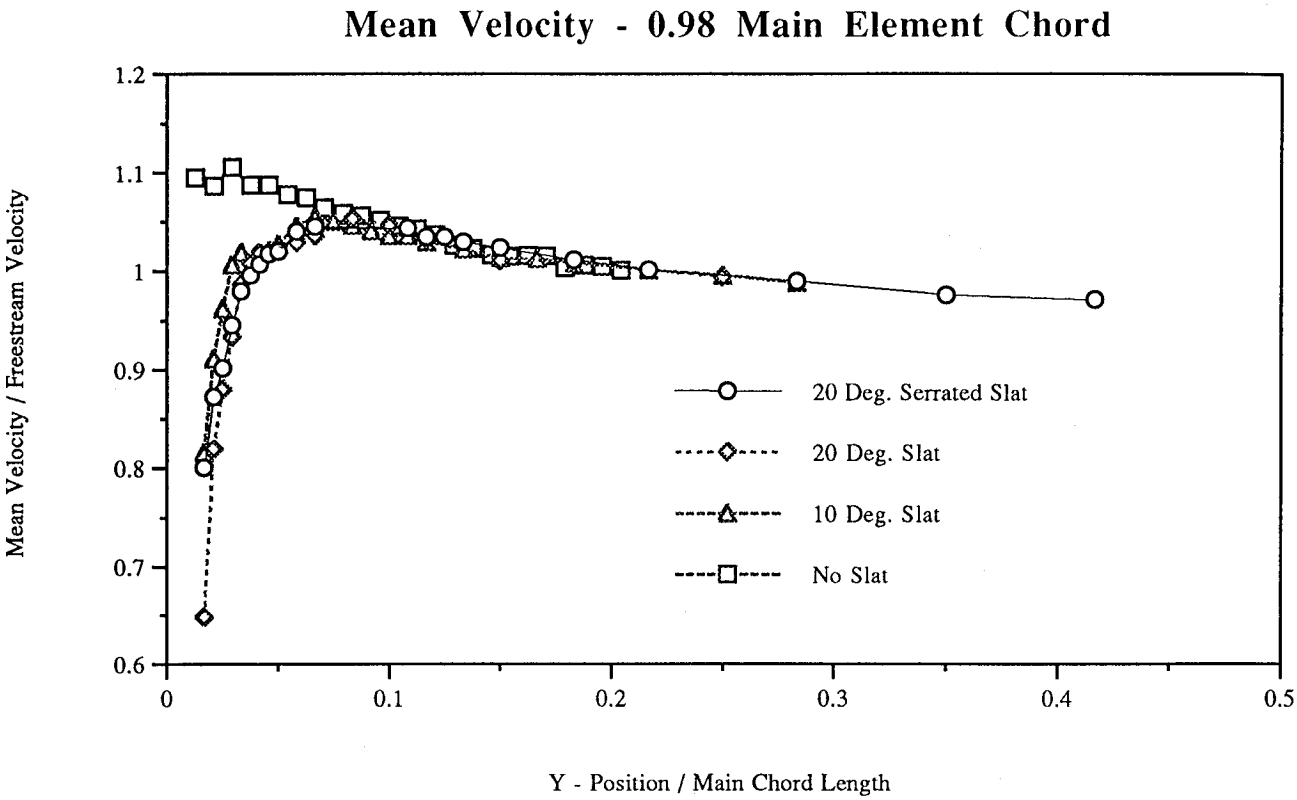
Mean Velocity - 0.98 Main Element Chord
Mean Velocity / Freestream Velocity
1.2
1.1
1
0.9
0.8
0.7
0.6
0
0.1
0.2
0.3
0.4
0.5
20 Deg. Serrated Slat
20 Deg. Slat
10 Deg. Slat
No Slat
Y - Position / Main Chord Length

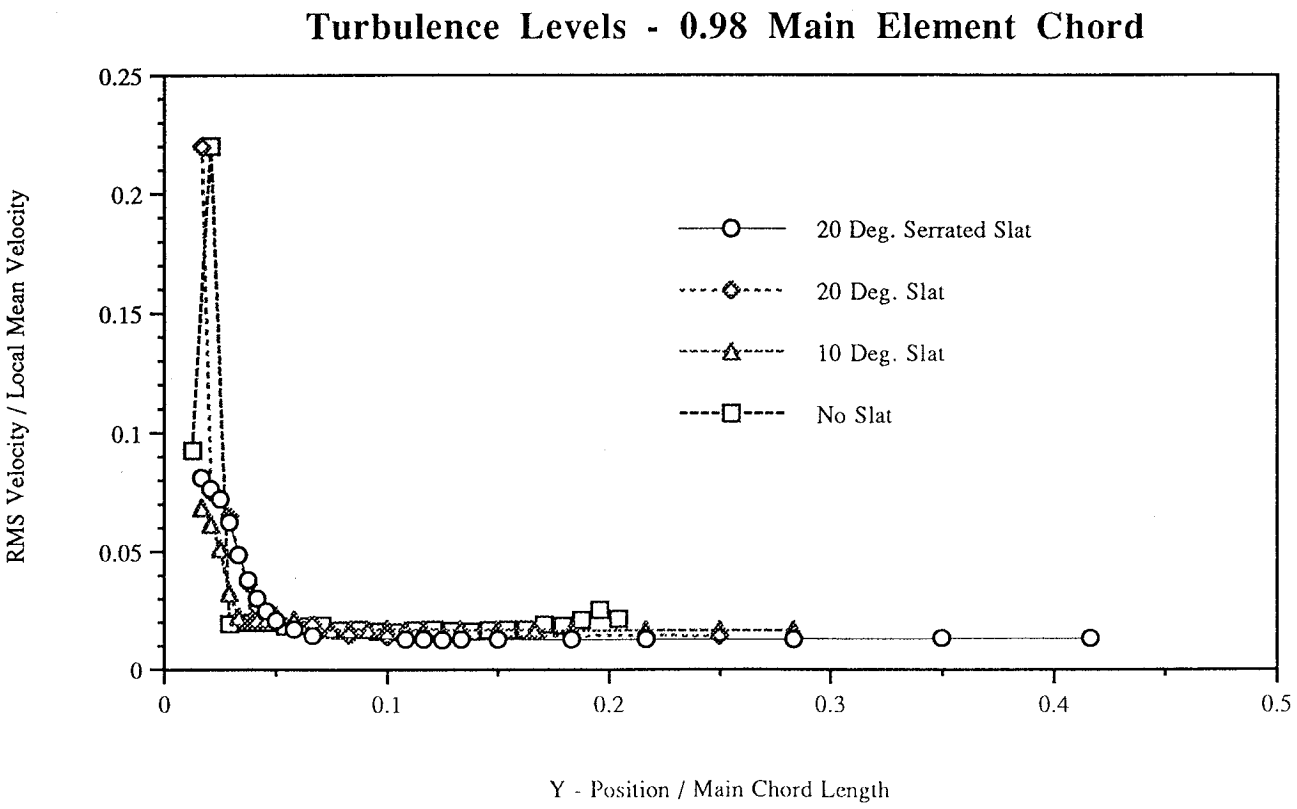
Turbulence Levels - 0.98 Main Element Chord
RMS Velocity / Local Mean Velocity
0.25
0.2
0.15
0.1
0.05
0
0
0.1
0.2
0.3
0.4
0.5
20 Deg. Serrated Slat
20 Deg. Slat
10 Deg. Slat
No Slat
Y - Position / Main Chord Length

Figure 9

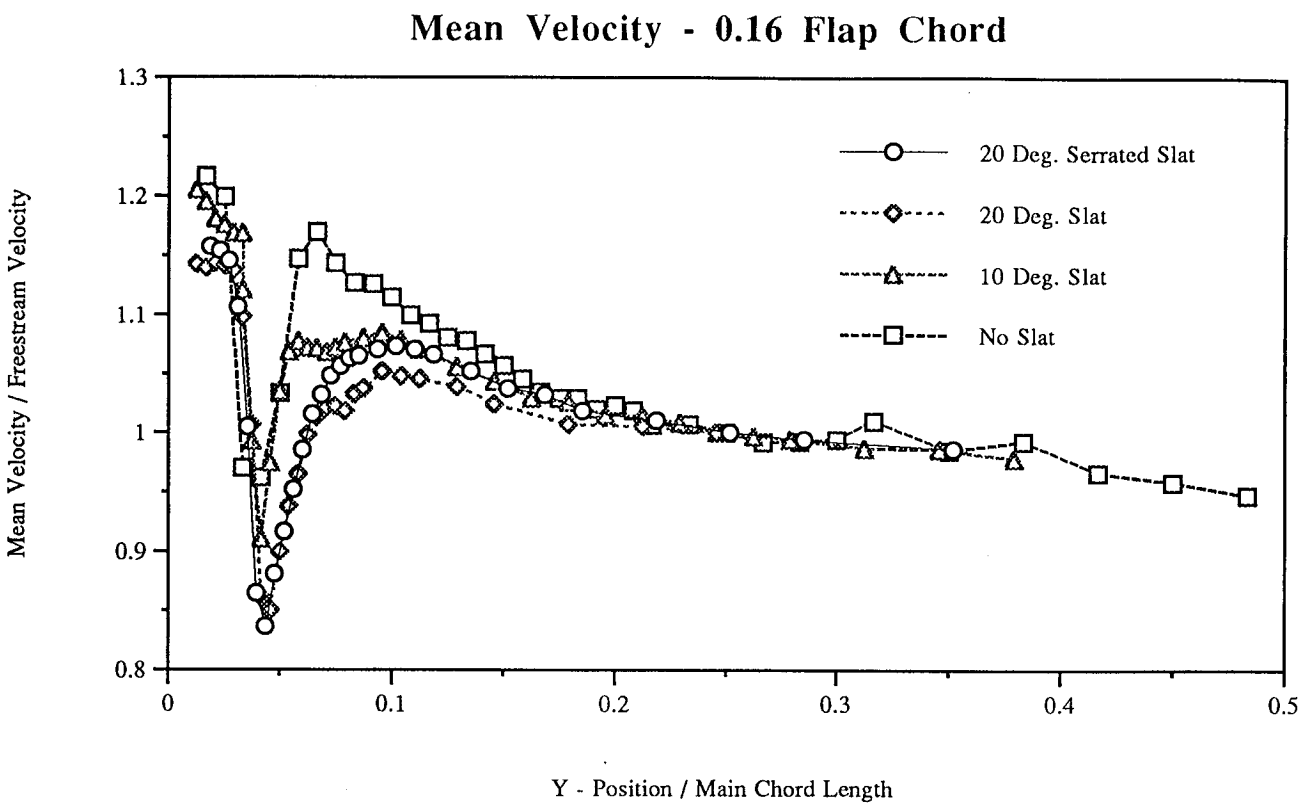
Mean Velocity - 0.16 Flap Chord
Mean Velocity / Freestream Velocity
1.3
1.2
1.1
1
0.9
0.8
0
0.1
0.2
0.3
0.4
0.5
20 Deg. Serrated Slat
20 Deg. Slat
10 Deg. Slat
No Slat
Y - Position / Main Chord Length

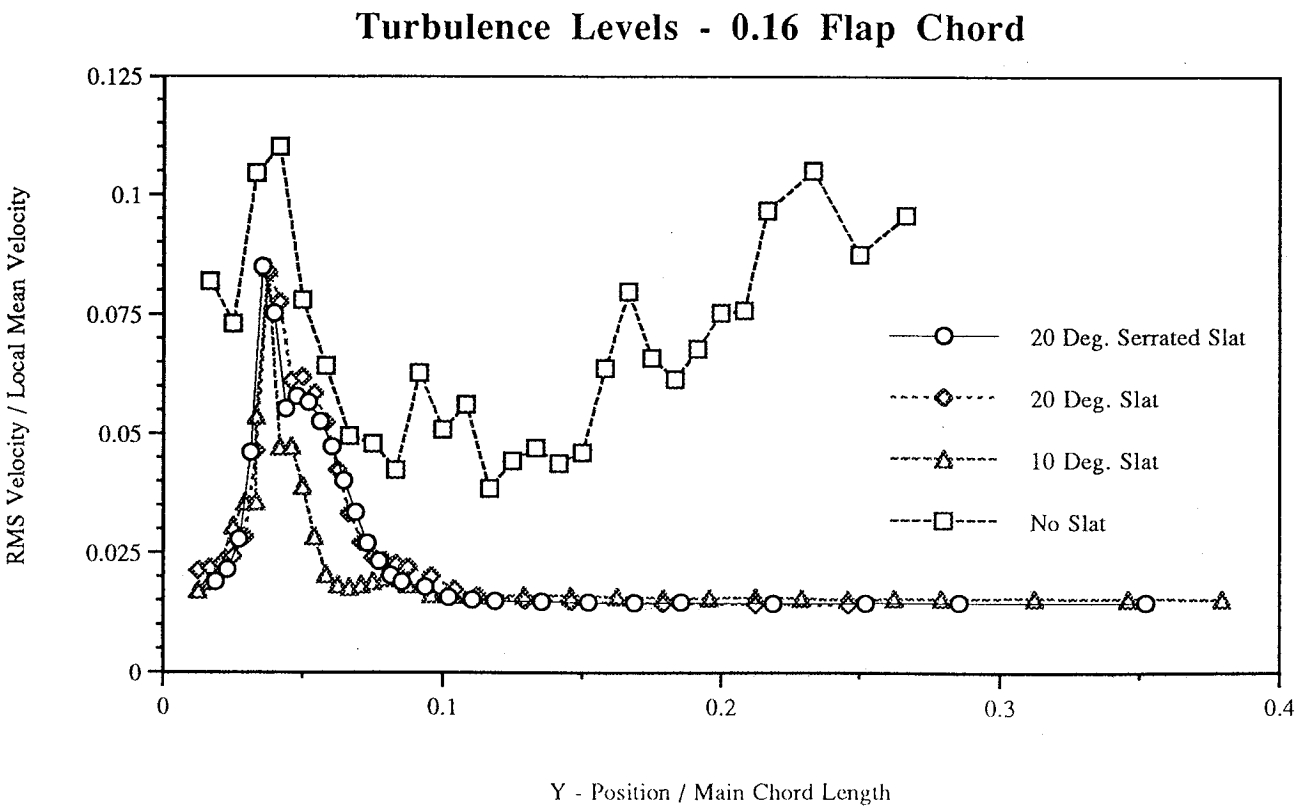
Turbulence Levels - 0.16 Flap Chord
RMS Velocity / Local Mean Velocity
0.125
0.1
0.075
0.05
0.025
0
0
0.1
0.2
0.3
0.4
20 Deg. Serrated Slat
20 Deg. Slat
10 Deg. Slat
No Slat
Y - Position / Main Chord Length

Figure 10

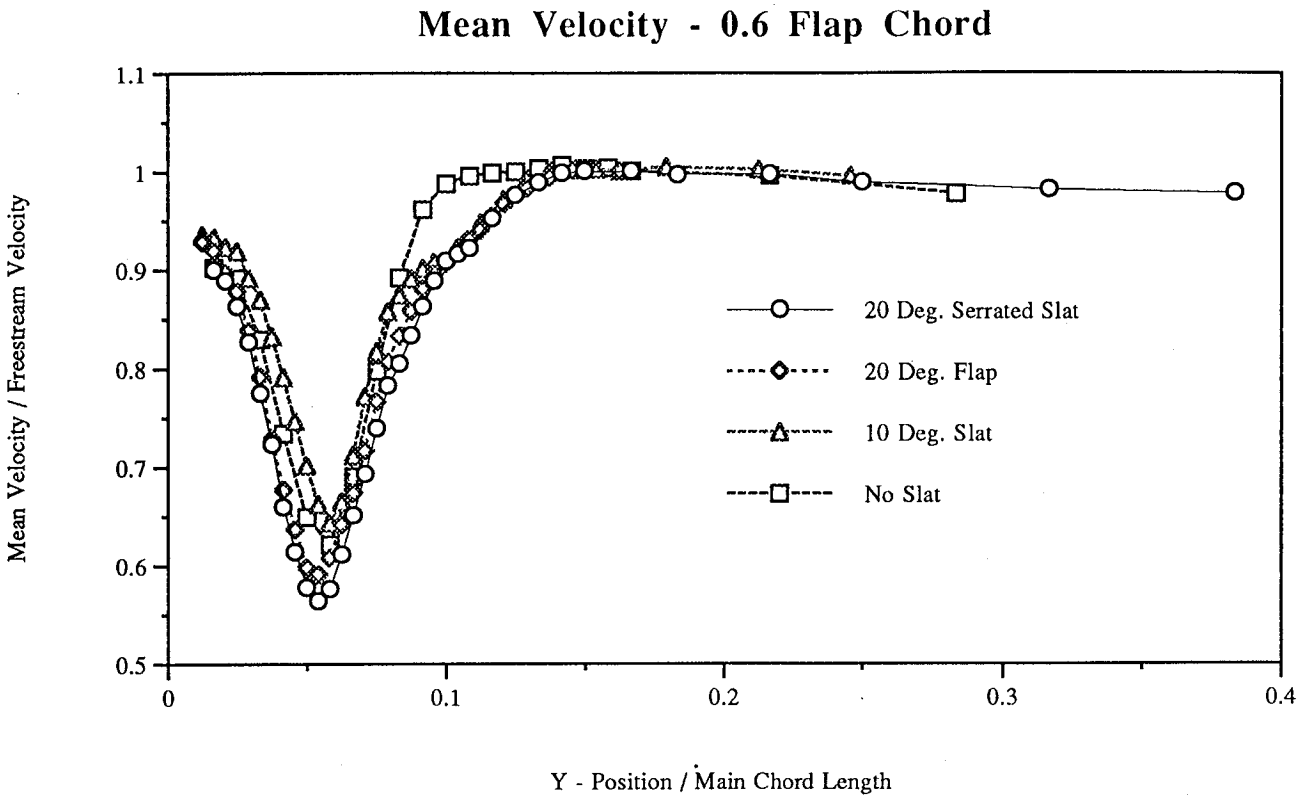
Mean Velocity - 0.6 Flap Chord
Mean Velocity / Freestream Velocity
1.1
1
0.9
0.8
0.7
0.6
0.5
0
0.1
0.2
0.3
0.4
20 Deg. Serrated Slat
20 Deg. Flap
10 Deg. Slat
No Slat
Y - Position / Main Chord Length

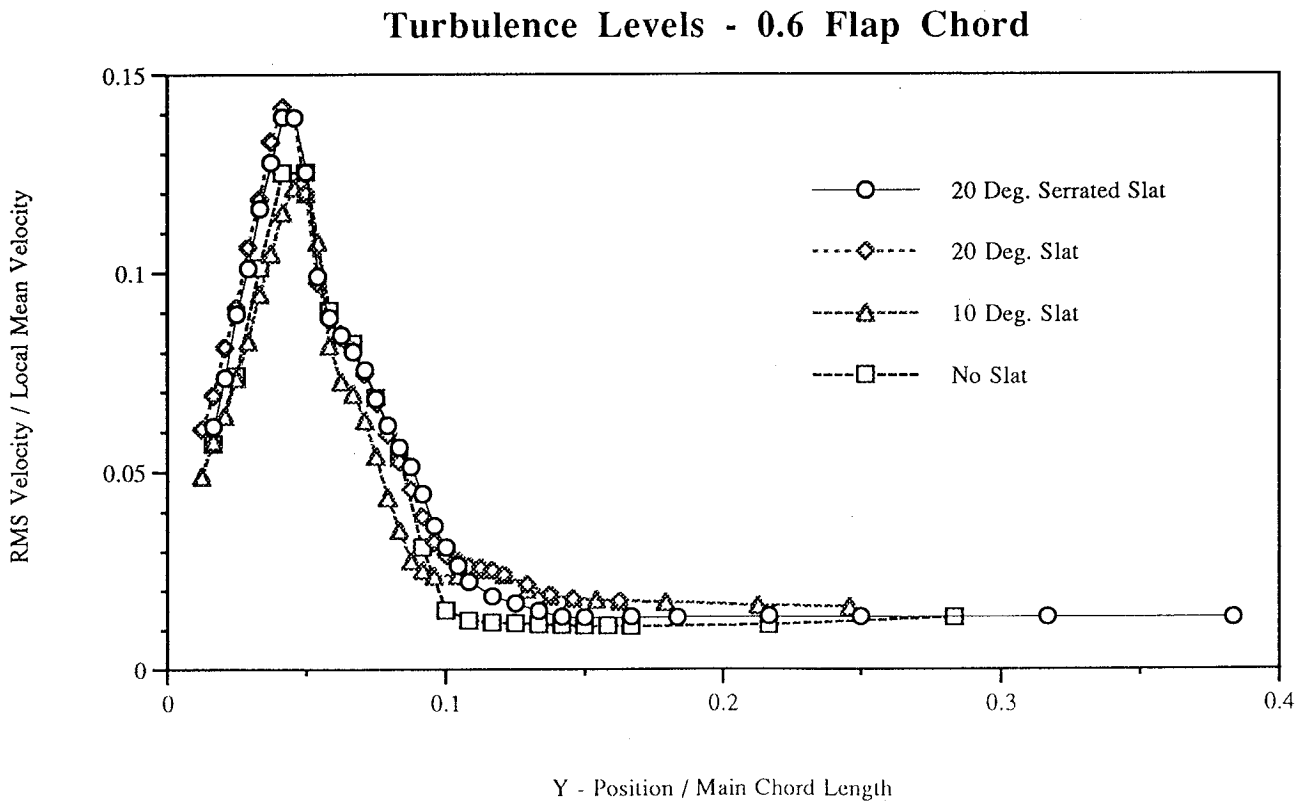
Turbulence Levels - 0.6 Flap Chord
RMS Velocity / Local Mean Velocity
0.15
0.1
0.05
0
0
0.1
0.2
0.3
0.4
20 Deg. Serrated Slat
20 Deg. Slat
10 Deg. Slat
No Slat
Y - Position / Main Chord Length

Figure 11

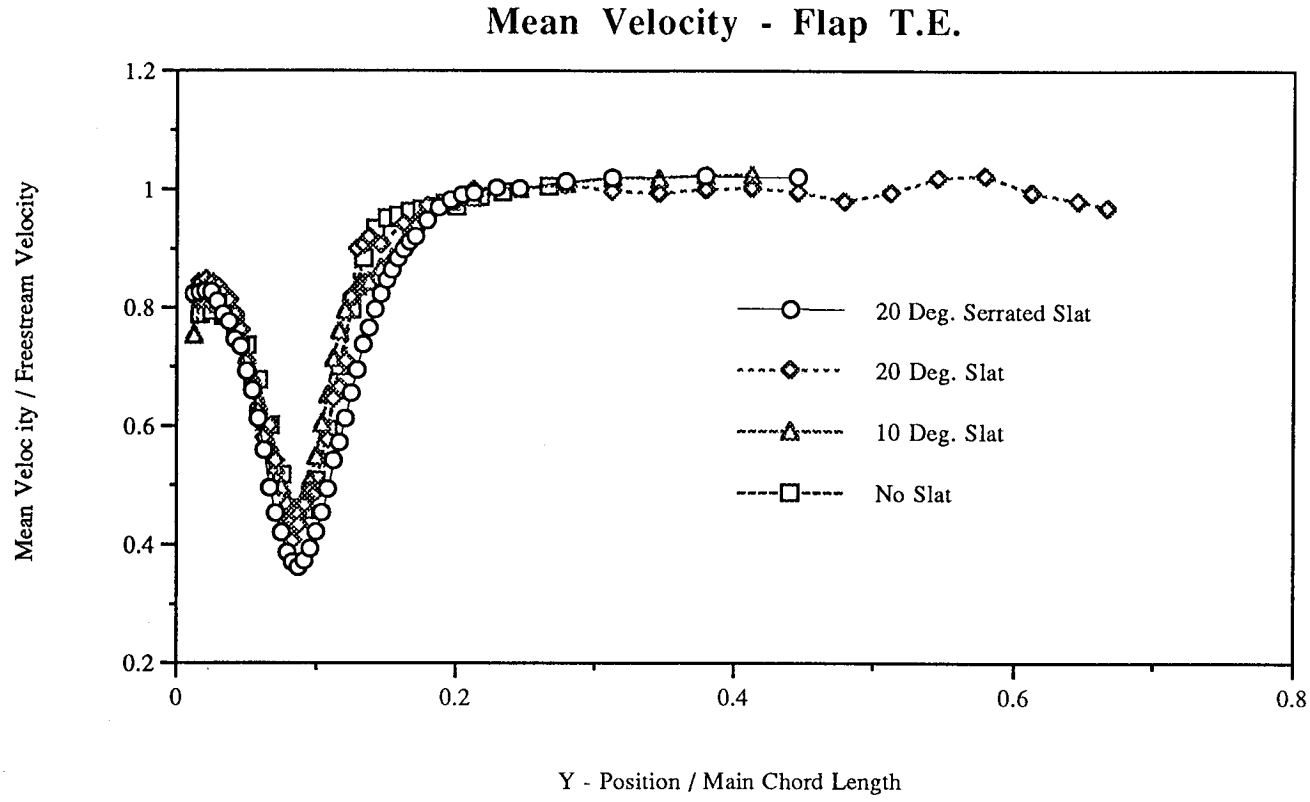
Mean Velocity - Flap T.E.
Mean Veloc ity / Freestream Velocity
1.2
1
0.8
0.6
0.4
0.2
0
0.2
0.4
0.6
0.8
20 Deg. Serrated Slat
20 Deg. Slat
10 Deg. Slat
No Slat
Y - Position / Main Chord Length

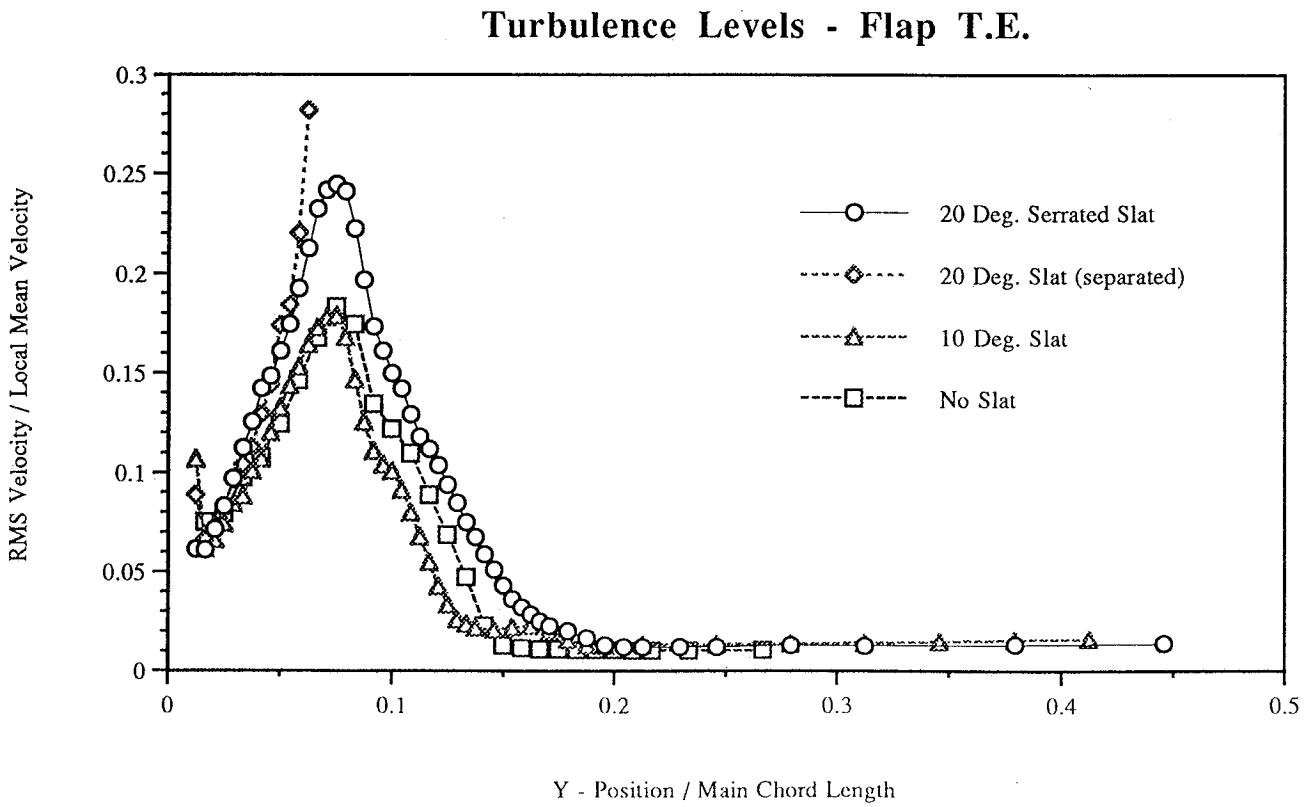
Turbulence Levels - Flap T.E.
RMS Velocity / Local Mean Velocity
0.3
0.25
0.2
0.15
0.1
0.05
0
0.1
0.2
0.3
0.4
0.5
20 Deg. Serrated Slat
20 Deg. Slat (separated)
10 Deg. Slat
No Slat
Y - Position / Main Chord Length

Figure 12

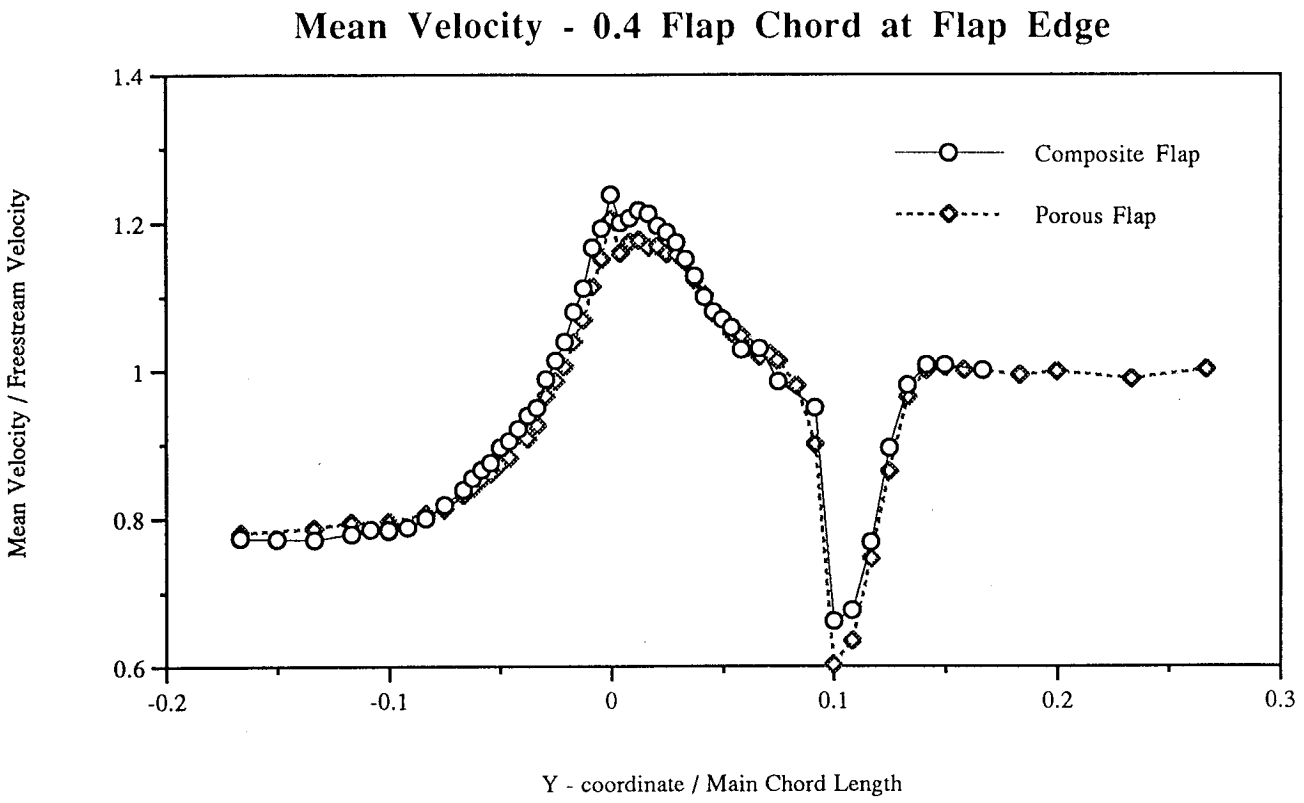
Mean Velocity - 0.4 Flap Chord at Flap Edge
Mean Velocity / Freestream Velocity
1.4
1.2
1
0.8
0.6
-0.2
-0.1
0
0.1
0.2
0.3
Composite Flap
Porous Flap
Y - coordinate / Main Chord Length

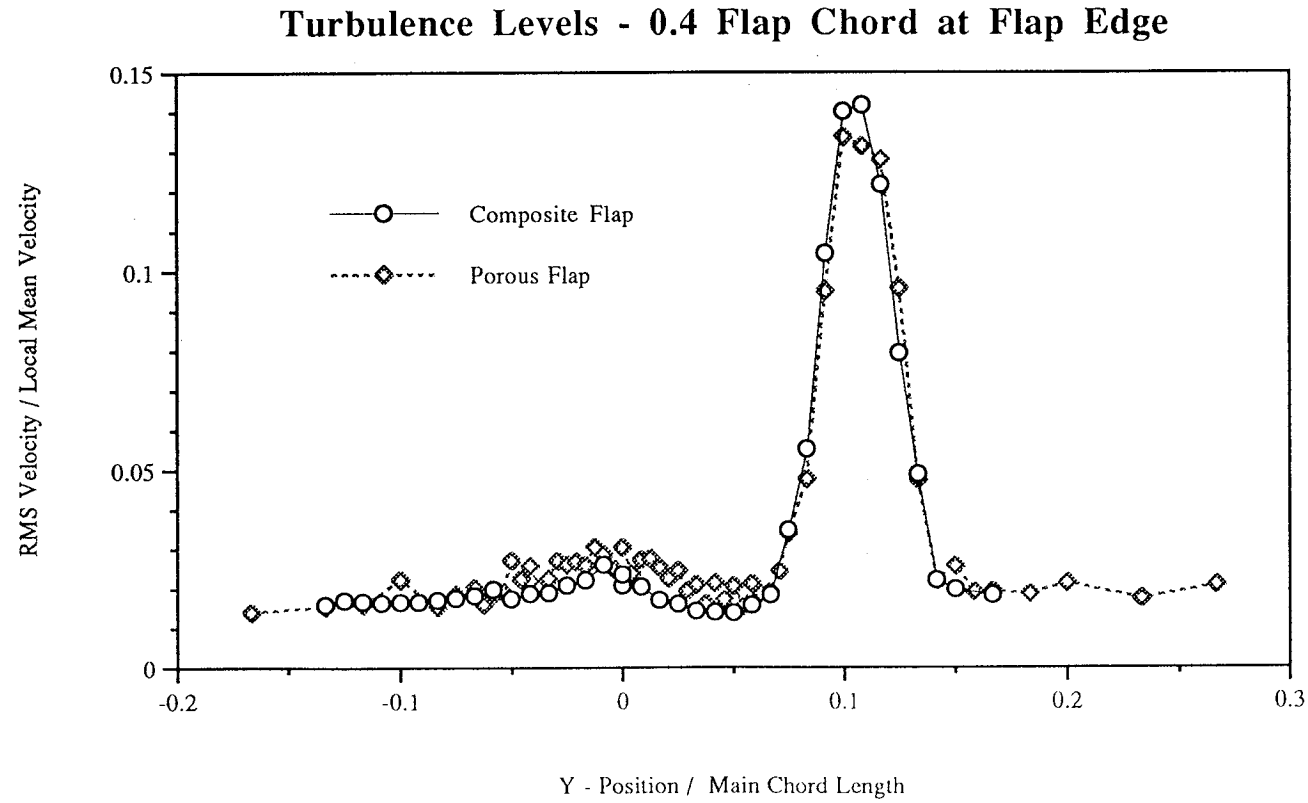
Turbulence Levels - 0.4 Flap Chord at Flap Edge
RMS Velocity / Local Mean Velocity
0.15
0.1
0.05
0
-0.2
-0.1
0
0.1
0.2
0.3
Composite Flap
Porous Flap
Y - Position / Main Chord Length

Figure 13

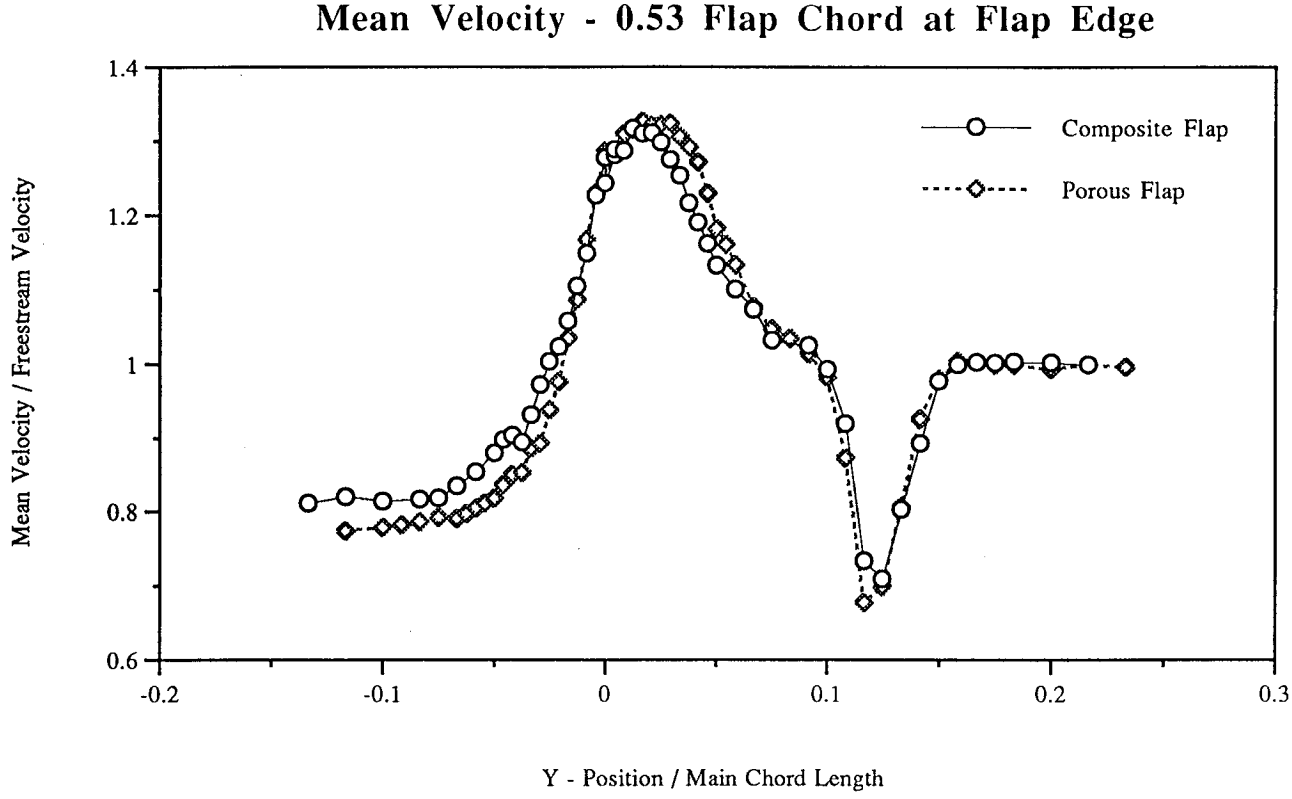
Mean Velocity - 0.53 Flap Chord at Flap Edge
Mean Velocity / Freestream Velocity
1.4
1.2
1
0.8
0.6
-0.2
-0.1
0
0.1
0.2
0.3
Composite Flap
Porous Flap
Y - Position / Main Chord Length

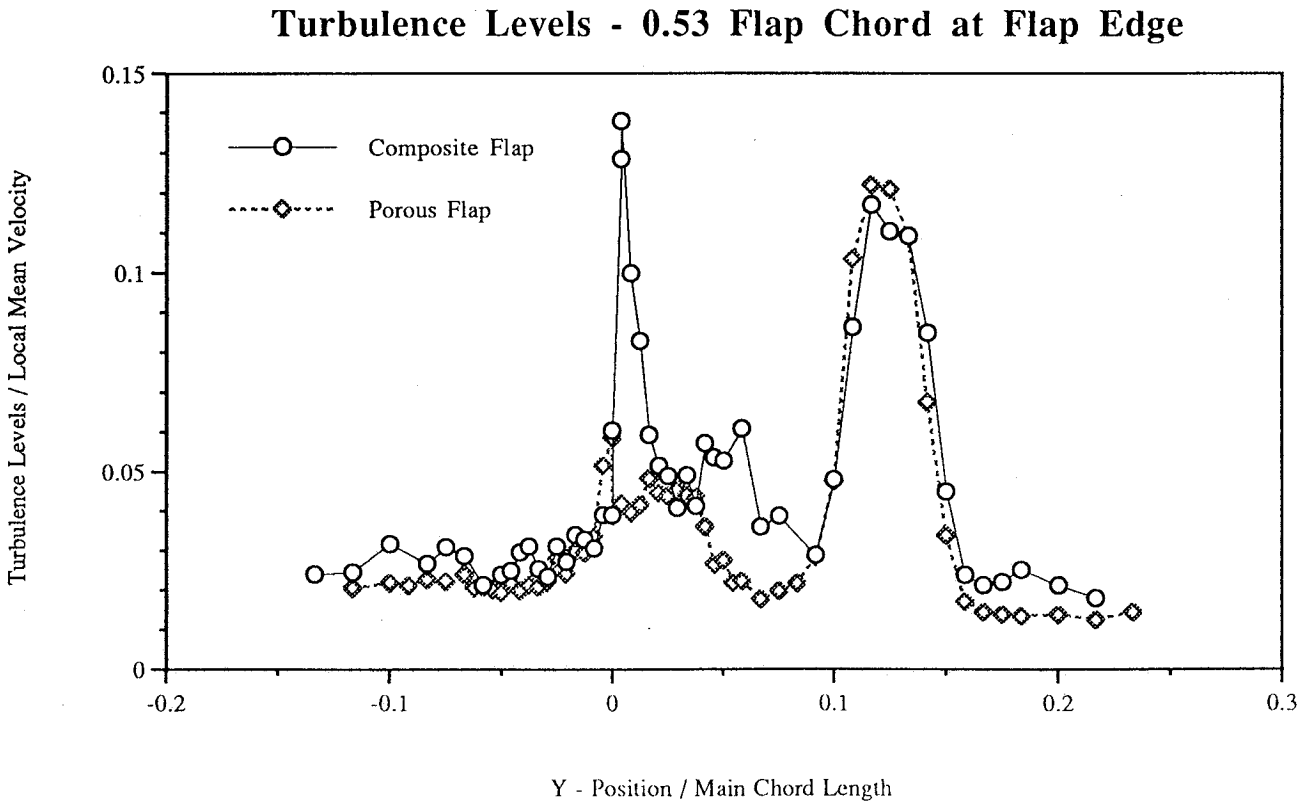
Turbulence Levels - 0.53 Flap Chord at Flap Edge
Turbulence Levels / Local Mean Velocity
0.15
0.1
0.05
0
-0.2
-0.1
0
0.1
0.2
0.3
Composite Flap
Porous Flap
Y - Position / Main Chord Length

Figure 14

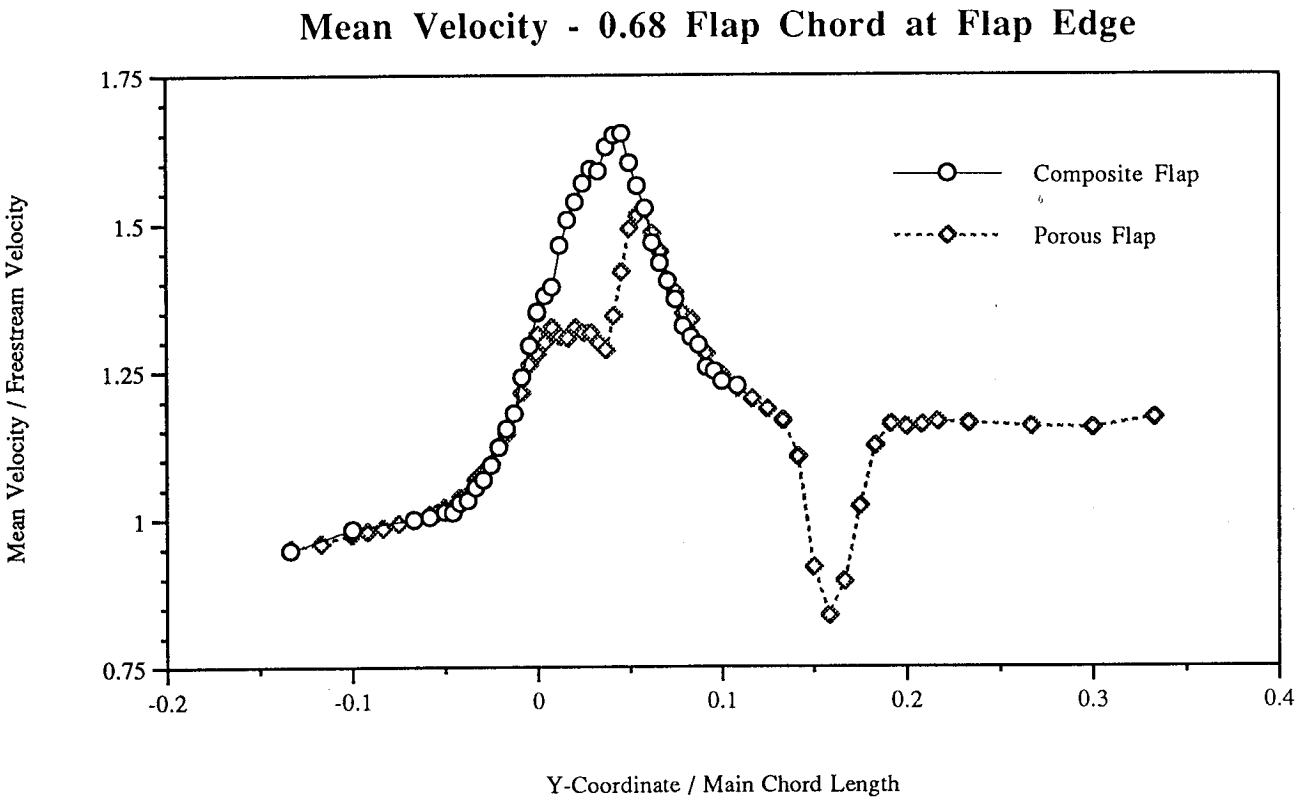
Mean Velocity - 0.68 Flap Chord at Flap Edge
Mean Velocity / Freestream Velocity
1.75
1.5
1.25
1
0.75
-0.2
-0.1
0
0.1
0.2
0.3
0.4
Composite Flap
Porous Flap
Y-Coordinate / Main Chord Length

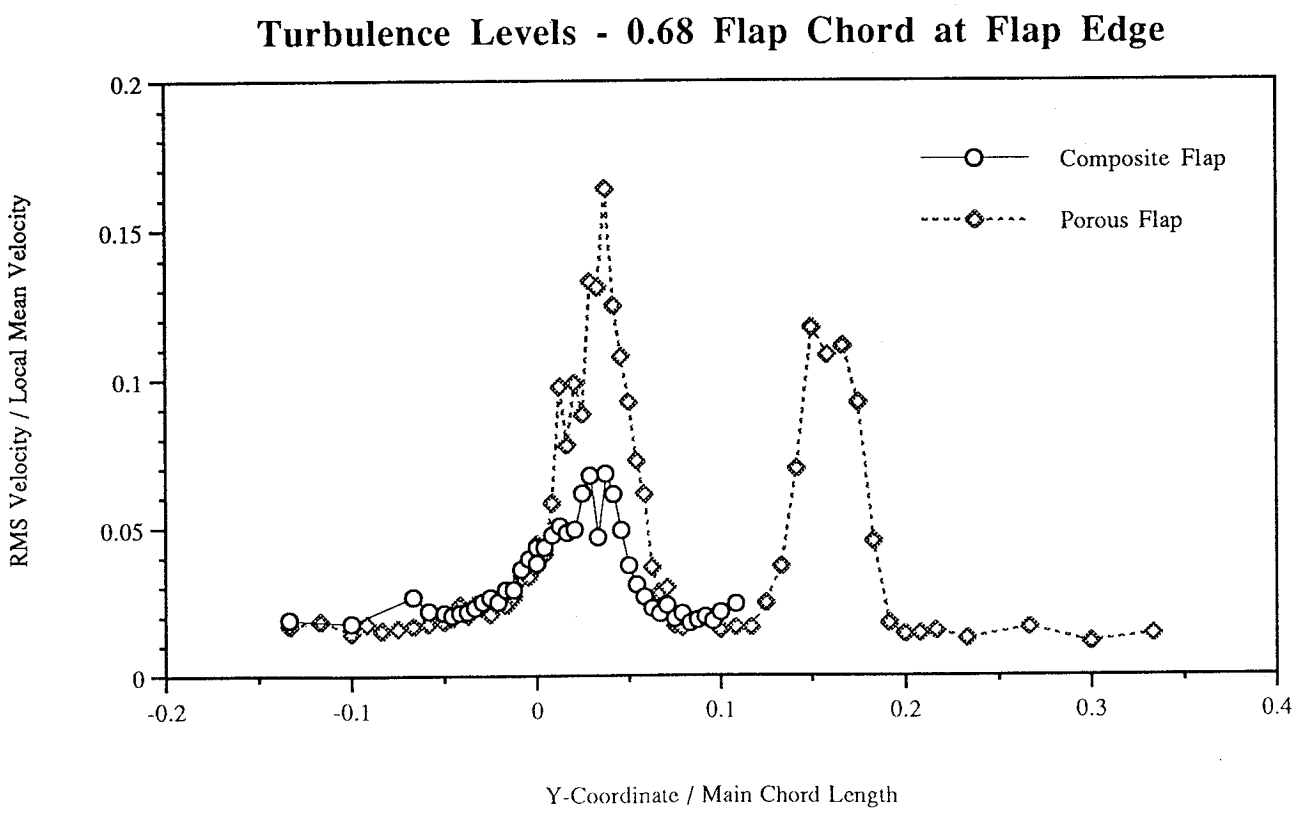
Turbulence Levels - 0.68 Flap Chord at Flap Edge
RMS Velocity / Local Mean Velocity
0.2
0.15
0.1
0.05
0
-0.2
-0.1
0
0.1
0.2
0.3
0.4
Composite Flap
Porous Flap
Y-Coordinate / Main Chord Length

Figure 15

Appendix A : Experimental Setup for Cylinder and Flap Edge Tests

Cylinder Test Setup

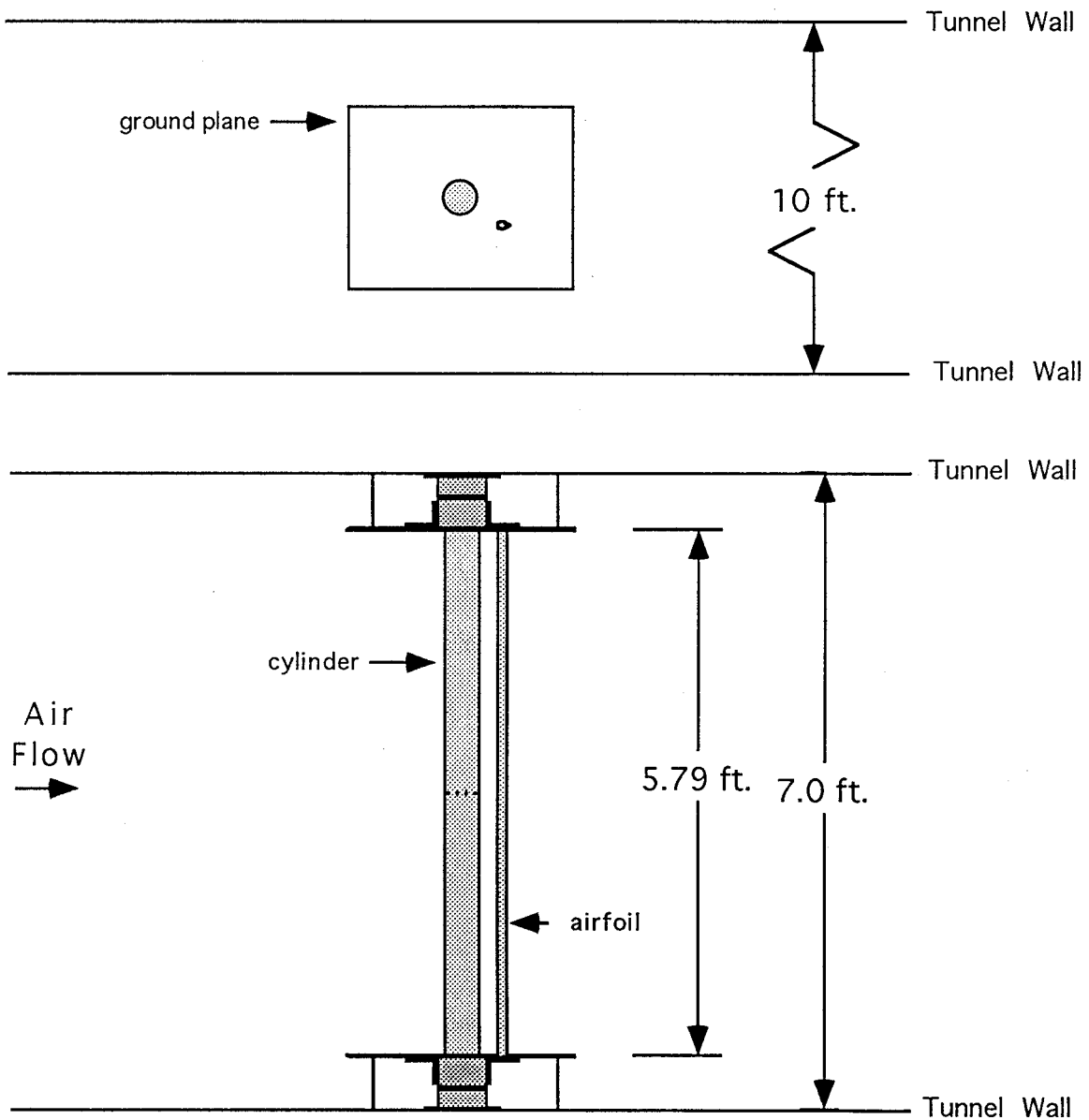

Position of Airfoil Section Relative to Cylinder

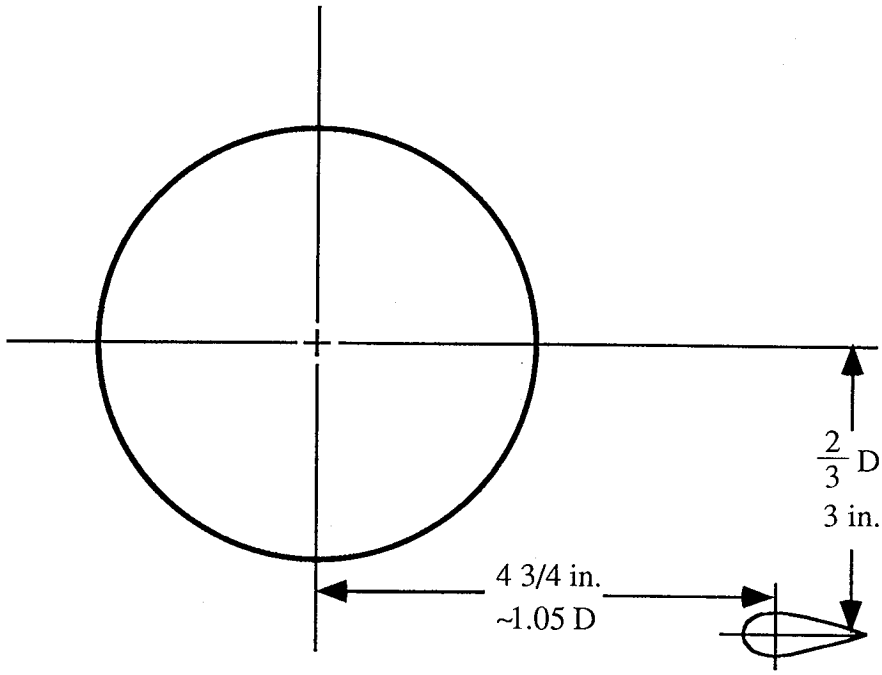

Wing Geometry with Hot-wire Measurement Planes

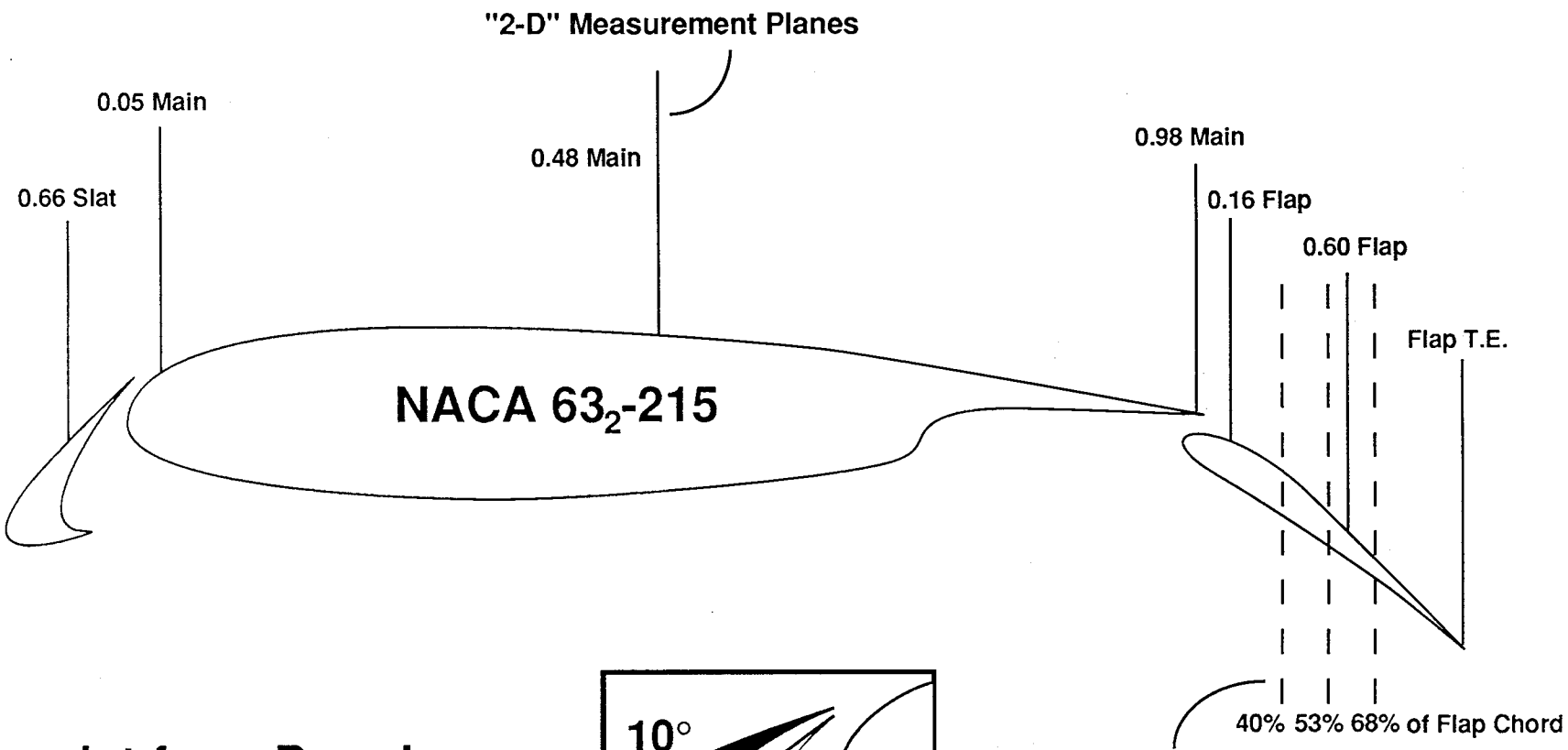

12%c slat from Douglas
3-element section (LB-546)

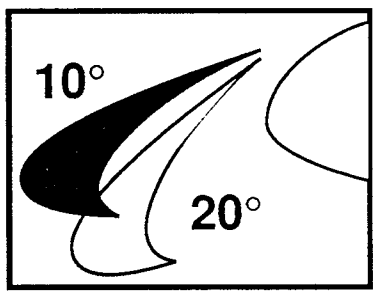

30%c Fowler flap

Top View of Wing with Hot-wire Measurement Planes